J Comput Aided Mol Des (2009) 23:807–828
DOI 10.1007/s10822-009-9299-7

Homology modelling of the human adenosine A_{2B} receptor based on X-ray structures of bovine rhodopsin, the β_2-adrenergic receptor and the human adenosine A_{2A} receptor

Farag F. Sherbiny · Anke C. Schiedel · Astrid Maaß · Christa E. Müller

Received: 3 February 2009 / Accepted: 12 August 2009 / Published online: 10 September 2009

Abstract A three-dimensional model of the human adenosine A_{2B} receptor was generated by means of homology modelling, using the crystal structures of bovine rhodopsin, the β_2-adrenergic receptor, and the human adenosine A_{2A} receptor as templates. In order to compare the three resulting models, the binding modes of the adenosine A_{2B} receptor antagonists theophylline, ZM241385, MRS1706, and PSB601 were investigated. The A_{2A}-based model was much better able to stabilize the ligands in the binding site than the other models reflecting the high degree of similarity between A_{2A} and A_{2B} receptors: while the A_{2B} receptor shares about 21% of the residues with rhodopsin, and 31% with the β_2-adrenergic receptor, it is 56% identical to the adenosine A_{2A} receptor. The A_{2A}-based model was used for further studies. The model included the transmembrane domains, the extracellular and the intracellular hydrophilic loops as well as the terminal domains. In order to validate the usefulness of this model, a docking analysis of several selective and nonselective agonists and antagonists was carried out including a study of binding affinities and selectivities of these ligands with respect to the adenosine A_{2A} and A_{2B} receptors. A common binding site is proposed for antagonists and agonists based on homology modelling combined with site-directed mutagenesis and a comparison between experimental and calculated affinity data. The new, validated A_{2B} receptor model may serve as a basis for developing more potent and selective drugs.

Keywords Homology modelling · Adenosine A_{2B} receptor · Docking · Antagonist · Agonist

Electronic supplementary material The online version of this article (doi:10.1007/s10822-009-9299-7) contains supplementary material, which is available to authorized users.

F. F. Sherbiny (✉) · A. C. Schiedel · C. E. Müller
PharmaCenter Bonn, Pharmaceutical Institute, Pharmaceutical Chemistry I, An der Immenburg 4, 53121 Bonn, Germany
e-mail: selim@scai.fraunhofer.de

F. F. Sherbiny · A. Maaß
Fraunhofer Institute SCAI, Schloss Birlinghoven, 53754 Sankt Augustin, Germany

Introduction

G protein-coupled receptors (GPCRs) constitute a prominent superfamily of drug targets [1]. Up to 50% of all modern-day medicines act on GPCRs [2]. GPCRs play a vital role in signal transduction and may be activated by a wide variety of ligands, including photons, amines, hormones, neurotransmitters and proteins. GPCRs are single polypeptide chains having seven hydrophobic transmembrane-spanning segments (7TM) that couple to an effector molecule through a trimeric G protein complex [3]. However, there is very little structural information available about this class of proteins as they are membrane proteins and thus difficult to crystallize. Some ligands bind to the extracellular loops of the receptors, while others penetrate into the transmembrane regions. In order to rationally design an effective drug to act on any given target protein knowledge of the three-dimensional (3D) structure of the target receptor is highly useful [4].

The adenosine receptors (ARs) are members of the superfamily of GPCRs belonging to the subfamily of rhodopsin-like receptors. Four adenosine receptor subtypes are known; these include the A_1 and A_3 receptors, which inhibit adenylate cyclase, and the A_{2A} and A_{2B} adenosine receptors, which stimulate adenylate cyclase [5]. Coupling to other second messenger systems, e.g. activation of K^+

channels (A_1), or phospholipase C (all subtypes) has been described [6]. The receptor subtypes can also be characterized according to the potency of the natural agonist adenosine: in most native systems the rank order of potency for adenosine is as follows: $A_1 \geq A_{2A} >> A_3 \approx A_{2B}$ [7], i.e. the A_1 and A_{2A} subtypes are high-affinity receptors activated by adenosine in nanomolar concentrations, while the A_{2B} and A_3 receptors are low-affinity subtypes that require high micromolar concentrations for activation. However, in artificial systems with high receptor expression at least the A_3 receptor can also be activated by low adenosine concentrations [6, 8].

Adenosine receptors are becoming important drug targets in the treatment of a variety of diseases because of their key roles in controlling physiological processes. Therapeutic agents under development include drugs for the treatment of central nervous system disorders (e.g. Parkinson's disease), inflammatory diseases, asthma, kidney failure, and ischemic injuries [7, 9]. The development of agonists for adenosine A_{2B} receptors could be useful for the treatment of cardiac diseases such as hypertension or myocardial infarction, and in the management of septic shock [10], whereas A_{2B} antagonists could have a role in the treatment of Alzheimer's disease, cystic fibrosis, type-II diabetes and especially asthma [11].

In view of this, the knowledge of the 3D structure of adenosine receptors could be of great benefit in the process of structure guided drug design. Consequently, since the first crystal structure of a GPCR had been solved in 2000, namely that of bovine rhodopsin [12], many efforts have been undertaken in the field of GPCR modelling, and especially homology modelling studies have been performed. Ivanov et al. [13] described a model of the human adenosine A_{2B} receptor and predicted binding modes for xanthine derivatives. In 2004 a refined crystal structure of rhodopsin was published [14] and in 2007 the crystal structure of a second GPCR, the human β_2-adrenergic receptor, was made available. The latter showed the same typical features as the rhodopsin structures, but presented individual features at the same time [14, 15]. Most recently, the structure of the human A_{2A} adenosine receptor has been determined [16]. As all crystallized GPCRs were in their inactivated ground states harbouring ligands, the general position of the binding site of this family of GPCRs can be located with good confidence in the upper half of the helical bundle. The sequence identity between the human A_{2A} and A_{2B} adenosine receptor subtypes amounts to 56%, i.e. the sequence similarity still remains relatively low, although higher than in bovine rhodopsin (23% identity) and the human β_2-adrenergic receptor (31% identity). Encouraged by the findings of Forrest, Tang and Honig [17, 18] that homology modelling is able to yield models with acceptable accuracy (2 Å RMSD for Cα-trace in transmembrane regions) already for template sequence identities of 30%, we applied this approach to our protein of interest based on all available targets. Indeed several examples in literature, suggest that homology modelling is a viable route to conduct, e.g. screening experiments by high throughput docking [19–21].

Thus in the present study, we created new, improved and refined homology models for the human adenosine A_{2B} receptor based on the crystal structures of rhodopsin (1U19.pdb), of the human β_2-adrenergic receptor (2RH1.pdb) and of the human adenosine A_{2A} receptor (3EML.pdb). As the three-dimensional structure of homology models for proteins with a low percentage of sequence similarity to the template protein are inevitably affected with uncertainties, we integrated extra information during construction of the 3D-model. Thus the modelling and validation process was guided by continually matching the modelling results with those from mutagenesis studies and ligand binding assays.

We here describe a comparison among the models based on bovine rhodopsin (A_{2B}-I), on the β_2-adrenergic receptor (A_{2B}-II) and on the A_{2A} adenosine receptor (A_{2B}-III). We use well-known A_{2A} and A_{2B} antagonists and agonists as well as mutagenesis data to probe the validity of the models with respect to consistence with experimental evidence. Additionally, the binding affinity and selectivity of these ligands are investigated.

Materials and methods

Molecular modelling

The original input sequences of the human adenosine receptors and the templates were retrieved from the Swiss-Prot database [22] and aligned using the ClustalW software [23]. The resulting preliminary alignment was manually refined to incorporate additional experimental evidence and avert gaps within the seven helical segments. Thus, the alignment was guided by the highly conserved amino acid residues (fingerprint motifs that are shared by the members of this family) including the extracellular disulfide bridge between TM3 and EL2, N1.50, D2.50, the E/DRY motif (D/E3.49, R3.50, and Y3.51), W4.50, the two proline residues P5.50 and P6.50, and the NPXXY motif (N7.49, P7.50, and Y7.53) [24] and in this respect is totally consistent with, e.g. the multiple alignment of all rhodopsin like sequences published in the GPCR-DB [25]. For the actual alignment, refer to the Supplementary Material (Fig. 1). In order to refer to the equivalent residues among different G protein-coupled receptors, we used the numbering system suggested by Ballesteros and Weinstein [26]. Information concerning the primary structure of the human adenosine A_{2B} receptor and the subdivision into transmembrane, cytoplasmatic and

extracellular domains was obtained from the GPCR Data Bank (GPCRDB, Information system for G protein-coupled receptors (GPCRs), www.gpcr.org).

The molecular models of the A_{2B} receptor were generated using the homology modelling service Homer (Homology modelling with homer. http://protein.cribi.unipd.it/homer/). Missing amino sequence parts were replaced by manually inserting glycines to obtain a complete backbone as a first step. The side-chains were subsequently substituted by the program SCWRL [27] according to the actual sequence. All models emerging from this procedure were minimized stepwise with respect to the force field energy by using the Amber package [28] to attain a low energy conformation. The minimization protocol consisted each of 2,400 cycles of the steepest descent algorithm followed by 1,400 cycles of the conjugated gradient method. Then the three models of the adenosine A_{2B} receptor were subjected to molecular dynamics simulation at 300 K during 400 ps. The geometrical parameters of the created models were evaluated and compared with those obtained for the native structure of the templates using the PROCHECK and PROSAII programs. The newly created 3D structures served as receptors for the subsequent docking experiments.

Docking studies

The molecular docking of a set of adenosine A_{2A} and A_{2B} antagonists and agonists was to be performed. Therefore, an automated docking procedure employing the FlexX software [29, 30] and the MD-package Amber was used to create suitable starting structures for subsequent molecular dynamic simulations (MD) in an attempt to improve the binding mode and predict the energetically most favourable binding mode for the respective ligand.

The following outlines our basic strategy in selecting the final conformation of each complex. Firstly, the geometry of the ligands was optimized by energy minimization using the Amber program. The compounds were automatically docked into the respective binding site, generally yielding several hundred diverse placements of the ligand. Each prediction was tested and finally reranked with respect to the force field energy by subjecting the whole system, i.e. the respective ligand complexed to the protein, to an energy minimization. In order to find the most relevant placements, we then performed a clustering analysis, as follows: of all not yet categorized conformations, the most favourable one served as reference for calculating the RMSD to every other conformation. Those conformations with an RMSD of less than 2.0 Å where neglected, from the others the one with the lowest value of force field energy became the new reference.

This was done until the originally very large set was reduced to only 10–20 diverse binding modes. In our experience it was sufficient to subject only the five most favourable candidates to the time-consuming further analysis of settling the ligand position and estimating the protein–ligand interactions.

Although the interaction energy between the ligand and the receptor may be very sensitive to subtle changes in the binding mode, here a threshold of 2.0 Å was considered appropriate in order to limit the number of conformations needing further analysis, as the dynamic motions during the subsequent MD-simulation were supposed to correct minor misplacements. In fact, by crossing over from rigid docking to molecular dynamics we not only switched from simple empirical scoring function to a more detailed energy function, but also allowed the ligand to accommodate to the protein surrounding and vice versa.

The following procedure for estimating the binding energy comprised a new step of energy minimization (1,500 steepest descent steps, followed by 500 of conjugate gradient until a convergence of 0.05 kJ mol^{-1} A^{-1} was reached), this time imposing no restraints at all. Then an MD-simulation was carried out, i.e. a total of 1 ns were recorded at 300 K, using a distance-dependent dielectric constant of $\varepsilon = 4r$ throughout all simulations in order to account for solvent screening. The MD-simulations were performed at 300 K, with a time-step of 1.0 fs. From the latter set of binding modes the candidate with the most favourable binding energy, which at the same time was in agreement with mutagenesis data, was accepted as final placement.

The binding energies between the receptor and the ligand were calculated on the basis of the Linear Interaction Energy approach originally proposed by Åquist and coworkers [31]. Accordingly, the binding free energy is approximated as the difference of the averaged nonbonded energies of the separate ligand and receptor from the nonbonded energy ofthe receptor–ligand complex: $\Delta G_{bind} = \alpha\left(\left\langle E^{elec}\right\rangle_{bound} - \left\langle E^{elec}\right\rangle_{free}\right) + \beta\left(\left\langle E^{vdw}\right\rangle_{bound} - \left\langle E^{vdw}\right\rangle_{free}\right)$, where the nonbonded energy is composed of an electrostatic part (including polar and nonpolar solvation) as well as a van der Waals part. Both parts may be weighed differently by the factors α and β, which may range from 0.169 to 0.5 in case of α and from 0.016 up to 1.043 for β [32, 33]. The exact values apparently depend on the protein under investigation.

As homology models are being created for lack of structure information, inevitably some uncertainty is inherent to the resulting 3D structures by nature, despite all efforts to compensate for this. Therefore, we did abstain from adjusting the parameters α and β such that they would match the experimental binding free energies as closely as possible and did apply $\alpha = \beta = 0.5$, thus neither preferring one nor the other. Therefore, the computed absolute values overestimate the binding affinity at least by a factor of 2–3. Moreover, changes in entropy are not sufficiently taken into

account, so that in consequence, the computed interaction energy values cannot be expected to reproduce exactly the experimental binding affinities. However, provided that the systematic errors are comparable among the ligands tested, the trend in binding affinity can be assessed by relating our results to observed K_i values via the equation $\Delta G = -RT \ln K_i$, which already would help to distinguish between good and bad ligand candidates.

Results and discussion

Homology modelling

The sequences of all human adenosine receptors were aligned to those of the templates in order to identify the amino acid residues that putatively form the seven transmembrane α-helices of the adenosine A_{2B} receptor. Three homology models were obtained for the adenosine A_{2B} receptor based on published X-ray structures of GPCRs. A particular difficulty with GPCRs in terms of computational complexity relates to the fact that GPCRs are membrane proteins and depend strongly in their conformational stability on their natural surrounding. Hence, the model system of choice would comprise the protein, a membrane patch and layers of water as demonstrated, e.g. by Schlegel et al. [34]. However, we not only intended to create models, but also wanted to study their ligand binding behaviour, therefore we restricted our computations to a system of economic size, which comprised the protein, eventually a bound ligand compound and water caps at the intra- and extra-cellular regions. Thus, the membrane, which would exert most probably nondirected and weak dispersive interactions to the protein, was neglected. We accounted for the limitations inherent to this simplified approach by including experimental evidence where possible.

One of the most important anchor points in modelling the individual backbone course of hydrophilic loops is the presence of the disulfide bond between TM3 and EL2, which is highly conserved among all rhodopsin-like receptors [35]. In the obtained models the disulfide bond was formed between Cys78 and Cys171, which was confirmed by mutagenesis studies (S. Hinz, A. Schiedel, C. E. Müller, unpublished results) and corresponds to the Cys110–Cys187 disulfide bond in bovine rhodopsin, the Cys106–Cys191 disulfide bridge in the β_2-adrenergic receptor and the Cys77–Cys166 disulfide bridge in the adenosine A_{2A} receptor [14–16], respectively.

Three different models for the adenosine A_{2B} receptor were obtained using as templates either bovine rhodopsin, yielding the first model A_{2B}-I, an engineered GPCR, the β_2-adrenergic receptor, yielding model A_{2B}-II or the human adenosine A_{2A} receptor, yielding model A_{2B}-III (Fig. 1). The overall sequence identity between bovine rhodopsin and the human A_{2B} receptor amounts to 23%, while that between the β_2-adrenergic receptor and the human A_{2B} receptor amounts to 31%. In contrast, the sequence identity between the human A_{2A} and A_{2B} adenosine receptors amounts to 56%. As stated elsewhere, 30% of sequence identity is sufficient for creating an acceptable description of the binding site [18, 36]. The mere percentage of sequence identity between target and template, however, is not the only criterion for the final quality of the model.

The most striking difference between the individual template structures is reflected by the resulting models: in

Fig. 1 The homology models of the human adenosine A_{2B} receptor (*magenta*) are shown along with their templates (*yellow*): the left model, A_{2B}-I, is based on bovine rhodopsin (1U19.pdb), the model in the center, model A_{2B}-II, is based on the β_2-adrenergic receptor (2RH1.pdb), whereas the right one, model A_{2B}-III, is based on the adenosine A_{2A} receptor (3EML.pdb)

the A_{2B}-II model the extracellular portions of the TM1 and TM3 point away from the center of the receptor, TM4 is twisted away from the center of the receptor, TM5 is closer to the center of the receptor and TM6 is twisted away from the receptor on the cytoplasmic end when compared to A_{2B}-I. Moreover, the A_{2B}-II model has a short helical segment in the middle of the second extracellular loop (EL2), which is not present in the structure derived from bovine rhodopsin. The largest difference concerns helix 1, which lacks the proline-induced kink found in rhodopsin and thus is comparatively straight [15]. On the other hand, in the A_{2B}-III model most of the structural divergence arises in the extracellular portions of helices I, II, and V, where the variation in the position of helices II, III and V appears to redefine the location of the ligand binding pocket [16].

Criteria for pre-estimating the template quality may be based on the alignment score, the number and distribution of gaps, the length of sequence similarity and conservation of aligned amino acids as well as the number and length of insertions and deletions. Finally, the quality of the X-ray structures in terms of resolution and authenticity has to be considered as well.

The exactitude of the predictions by comparative modelling greatly depends on the degree of sequence similarity. If the target and the template share more than 50% of their sequences, predictions usually are of high quality. In our case, the alignment scores were 79.0 bits (193) for bovine rhodopsin, 96.7 bits (239) for the β_2-adrenergic and 267 bits (683) for the adenosine A_{2A} receptor. The gap ratio in the alignment of the human adenosine A_{2B} receptor with the β_2-adrenergic receptor was slightly worse ($26/217 = 11\%$) than that with bovine rhodopsin ($32/302 = 10\%$) but with the adenosine A_{2A} receptor ($10/215 = 4\%$) it was considerably much better (obtained by using the BLAST program; http://www.ncbi.nlm.nih.gov/blast/Blast.cgi?CMD=Web&PAGE_TYPE=BlastHome).

Concerning the quality of the crystal structures, we must consider that in order to facilitate the growth of diffraction-quality crystals, the human β_2-adrenergic was modified by inserting T4 lysozyme (T4L). However, according to Rosenbaum et al. [37] the engineered receptor did retain its basic functionality despite the structural modification: the agonist binding affinities were slightly elevated; the antagonist binding affinities remained almost unchanged. Thus, although displaying an engineered protein, the crystal structure represents a functional protein. Said 3D structure was solved at 2.4 Å resolution and in the presence of the antagonist carazolol, which points to the potential location of the ligand binding site. Yet, the N-terminus of the β_2-adrenergic receptor, especially the residues 1–28 and the majority of the C-terminus are not included in the crystal structure of the β_2-adrenergic receptor [15]. Conversely, the X-ray structure of bovine rhodopsin contains the complete receptor, harbouring a retinal moiety, at a slightly better resolution of 2.20 Å with a similar R-value of 0.200 [14]. The structure of the adenosine A_{2A} receptor was resolved at 2.6 Å resolution with a R-value 0.198. According to [18], a resolution of 2.5 Å implies that backbone as well as side-chain atoms are well resolved with an accuracy of ± 0.4 Å for the atomic positions. Thus all potential template structures are of comparable and supposedly sufficient quality.

Based only on the sequence relations the structure of the adenosine A_{2A} receptor would scores highest as a template. However, the sequence similarity might even turn out as a disadvantage, as the receptor was cocrystallized with ZM241385 and thus was accommodated to exactly this compound. Since we start with rigid docking, the binding site of a quite flexible receptor adapted to a given compound (or to none at all) might not be capable of accepting compounds of a different layout, at least this was found for protein kinases when testing crystal structures versus homology models [38, 39]. Considering this, as well as the authenticity and resolution of the crystal structures, the crystal structures of rhodopsin and the β_2-adrenergic receptor appear suited as well. Thus, at this point all crystal structures had to be considered as appropriate template structures for the adenosine A_{2B} receptor.

The formal validation of the created models was done with PROCHECK [40, 41] and PROSAII [42] to rule out gross errors, i.e. checking only the plausibility of the main chain and side-chain conformations with respect to allowed torsions, the absence of D-amino acids or *cis*-peptide conformations in each residue within the models. Whether the final models indeed do possess a realistic geometry and exert a certain predictive power was finally assessed by further docking and MD studies.

Accordingly, the plausibility of the final models was evaluated by means of Ramachandran's plots. As shown in Fig. 2 of the Supplementary Material, all helical amino acids are located in the region favouring a right-handed α-helix. Only 0.7% of all residues were in a sterically disallowed region in model A_{2B}-I, 1.7% of the respective residues were located in the disallowed region in model A_{2B}-II, while 0.7% of the respective residues were located in the disallowed region in model A_{2B}-III. In all cases these residues are located in loop segments, thus not affecting the core region of the models and therefore do not have to be corrected. The crystal template structures themselves did display 0.7, 0 and 0% of residues in disallowed regions in case of rhodopsin, the β_2-adrenergic receptor and the A_{2A} receptor, respectively.

The Z-score computed by PROSAII [42] indicates the overall model quality, and its value for the respective model is related to the Z-scores of all experimentally determined protein structures in the current database indicating whether

the Z-score of the particular structure is within the range of reasonable scores (Fig. 3, Supplementary Material). This plot shows the local model quality by plotting energies as a function of amino acid sequence position. In general, positive values correspond to problematic parts of the input structure. As a result, the bovine rhodopsin template shows a Z-score of −3.89 and the deduced model (A_{2B}-I) shows a Z-score of −3.07, the β_2-adrenergic receptor shows a Z-score of −2.6 and the derived model (A_{2B}-II) has a Z-score of −2.85, while the A_{2A} receptor shows a Z-score of −3.87 and the derived model (A_{2B}-III) has a Z-score of −4.19. These values indicate that the structural average for the second generation quality control values is within a normal range. Therefore all final refined models can be considered as suitable for further studies.

Firstly, a qualitative comparison of the common as well as of the individual structural features of all models was performed. The backbone root mean square deviation (RMSD) of the created models relative to the corresponding residues of the X-ray structures was calculated as a measure of structure similarity. As shown in (Fig. l) the trans-membrane parts, where the sequences match best, superimpose perfectly, whereas the backbone course of the extracellular and intracellular loop regions differ significantly from the original. This is most noticeable for the rhodopsin based model, as the N-terminus of the A_{2B} receptor is much shorter. Apart from a different arrangement of the helices, all models vary largely in the backbone course of EL2. While for the model A_{2B}-I a β-sheet conformation was assumed, the A_{2B}-II model inherited a short helix from the β_2-adrenergic receptor in this section. On the other hand, the A_{2B}-III model lacks the prominent secondary structural elements, such as β-sheet and α-helix, which were observed in the rhodopsin and β_2-adrenergic-based models.

Docking studies

With the aim of further validation, eventual selection of the best model and understanding the binding behaviour in terms of affinity as well as selectivity, we carried out several docking studies for a set of ligands as detailed in the methods section, and correlated the results to experimental studies.

The template structures accommodate their inactivating ligands geocentrically in a comparable position, i.e. in the outer half of the helix bundle. Therefore, the binding site of the models was transferred from the template structures to the models assuming that their mechanism of operation would be very similar.

Based on published studies, we collected a series of compounds to test the models of the human adenosine A_{2B} receptor (Figs. 2, 3). These compounds comprise 18 antagonists, as well as 7 agonists, addressing the inactive receptor state as well as the activated receptor conformation, as we wanted to exploit the predictive power of our model and methods, respectively. In detail, we included selective compounds besides unselective ones, xanthines as well as and non-xanthines, in order to identify the individual key features of the adenosine A_{2B} receptor that would allow to control it separately from the other subtypes and to be able to develop selective ligands by rational drug design. Most of the antagonist compounds investigated (**1**–**18**) are based on xanthine scaffolds (**1**–**12**), while other ligands show non-xanthine structures (**13**–**18**).

Docking of antagonists

Redocking of ZM241385 into the adenosine A_{2A} receptor

In order to check the efficiency of the method employed for creating suitable binding modes as described in the method section, we performed molecular redocking of ZM241385 [43] (compound **13** in Fig. 2) into the crystal structure of the A_{2A} receptor. As a result, the binding mode of ZM241385 with the A_{2A} receptor is similar to the reference (RMSD of 0.6 Å) where ZM241385 binds in an extended conformation and its orientation is almost perpendicular to the membrane plane, co-linear with transmembrane helix VII and interacting with both ECL2 and ECL3. In both structures, the bicyclic triazolotriazine core of the ligand is anchored by an aromatic stacking interaction with Phe168, aliphatic hydrophobic interactions with Ile274, Met177, Ile252, Met270 and Met174 and a hydrogen bonding interaction with Asn253.

Furthermore, Glu169 interacts with the exocyclic amino group, and the phenolic hydroxyl group forms a hydrogen bonding interaction with a water molecule. Also, the phenyl ring (this moiety appears to be mobile within the reference receptor) forms hydrophobic interactions with Leu267, Leu167, Tyr271 and His264 (Table 1). The furan ring is hydrogen-bonded to Asn253 and located in the hydrophobic pocket formed by His250, Leu85, Val84, and Leu249. Additionally, the furan ring is roughly 3.3 Å away from the highly conserved Trp246. We therefore conclude that indeed our docking and selection procedure successfully produces reasonable binding modes (Fig. 4).

Several antagonists were docked into the A_{2A} crystal structure (MSX-2, Istradefylline, Preladenant, MRS1706, MRE2029F20 and PSB-601)

In order to further assess the reliability of the method for estimating binding affinities. According to the experimental data MSX-2, Istradefylline, and Preladenant are A_{2A}

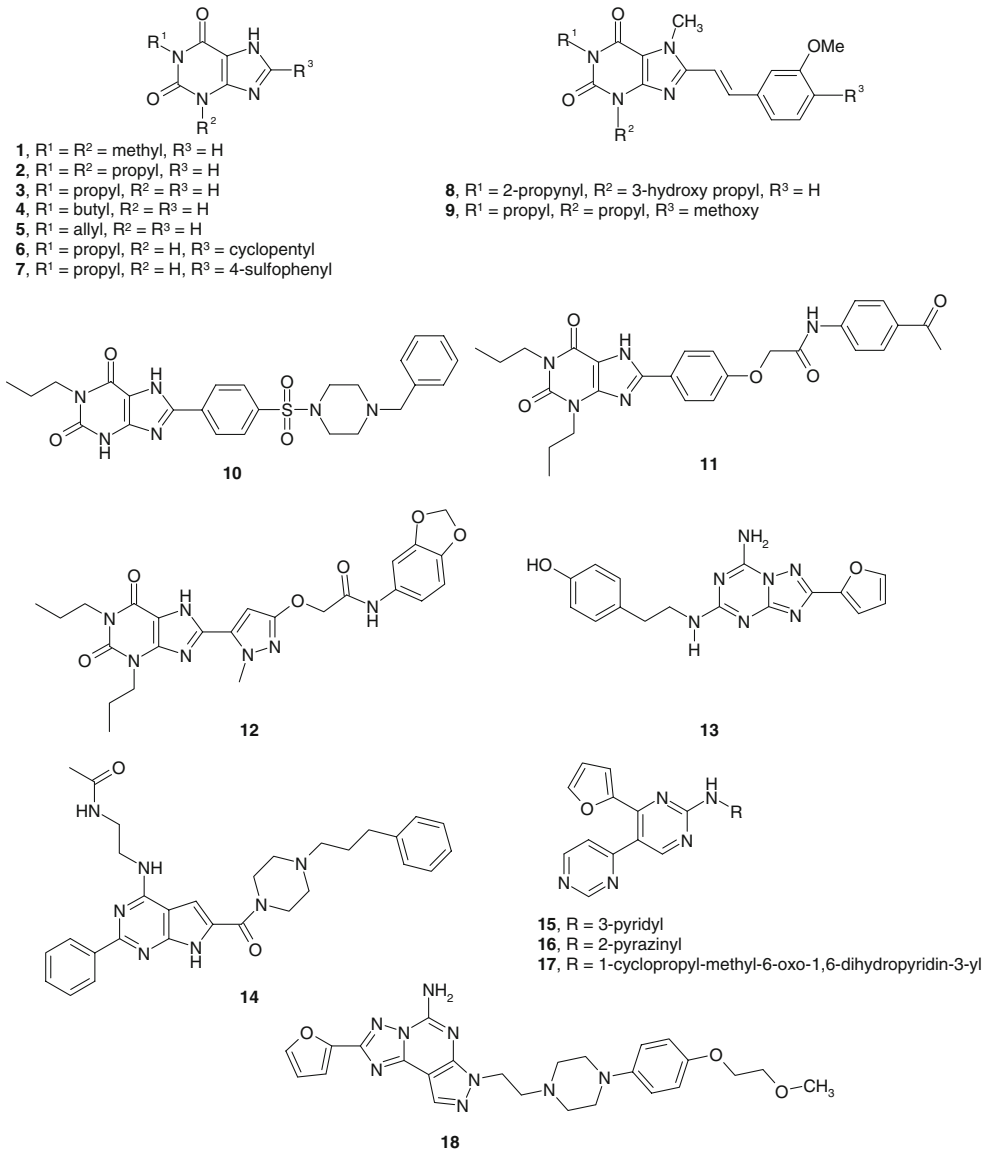

Fig. 2 Nonselective antagonists (**1**–**6**) and selective antagonists for the A_{2A} receptor (**8**, **9**, **13**, **18**) and selective antagonists (**7**, **10**–**12**, **14**–**17**) for the A_{2B} receptor (**1**, theophylline; **2**, 1,3-dipropylxanthine; **3**, 1-propylxanthine; **4**, 1-butylxanthine; **5**, 1-allylxanthine; **6**, 1-propyl-8-cyclopentylxanthine; **7**, PSB-1115; **8**, MSX-2; **9**, istradefylline; **10**, PSB-601; **11**, MRS1706; **12**, MRE2029F20; **13**, ZM241385; **14**, OSIP339391; **15**, **16**, and **17**, 2-aminopyrimidine derivatives; **18**, preladenant)

selective antagonists and display high binding affinities with K_i values 5.0, 13.0, and 1.1 nM for the A_{2A} receptor, whereas MRS1706, MRE2029F20 and PSB-601 are A_{2B} selective antagonists and show K_i values 112, >1,000, and 484 nM in the A_{2A} receptor. Based on mutagenesis data, a common binding mode for the compounds sharing a xanthine scaffold moiety is expected. As the binding affinities range from high to low, we anticipate finding the overall trend reflected in the calculated values. Indeed, all predictions display very similar placements of the xanthine moiety, which also coincides with the bicyclic core of ZM241385. The common interaction pattern involves Asn253 and Phe168.

The placement of the antagonist MSX-2 [44] (compound **8** in Fig. 2) illustrated in (Fig. 4) also shows a hydrogen bonding interaction between the carbonyl group at the 2-position of the ligand and Thr88, even though it is not maintained along the whole MD trajectory. The hydroxyl moiety of the ligand is stabilized by a hydrogen bonding interaction with the unprotonated nitrogen atom of His278 and the amino group at the 9-position of the ligand interacts with a water molecule. In addition, the methoxy oxygen atom of the ligand interacts with the backbone amino group of Phe168. Besides, the styryl moiety of the ligand is located in the hydrophobic pocket formed by Ala63, Ile66, and anchored by an aromatic stacking interaction with Tyr271.

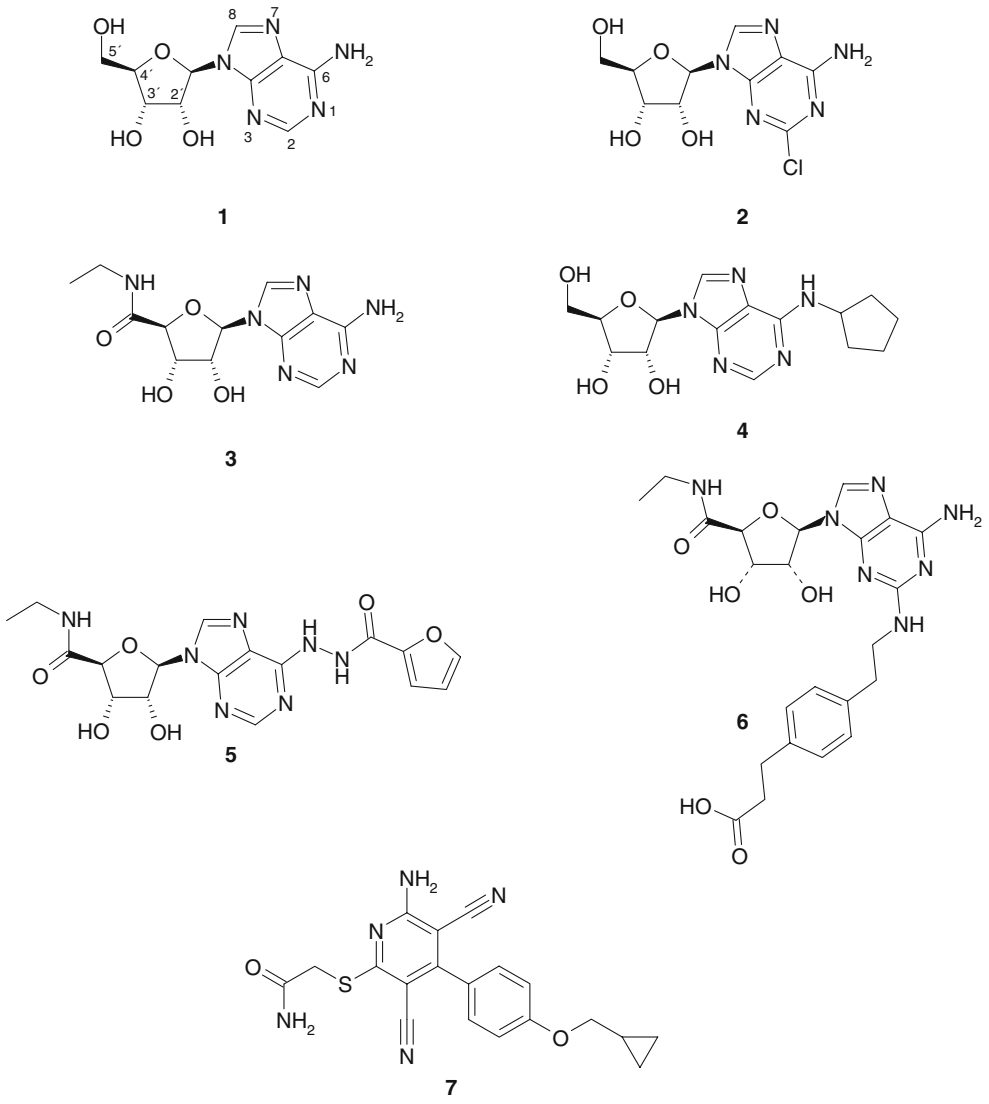

Fig. 3 Nonselective agonists (**1**–**4**), selective agonist for the A_{2A} receptor (**6**) and selective agonists (**5**, **7**) for the A_{2B} receptor (**1**, adenosine; **2**, CADO; **3**, NECA; **4**, CPA; **5**, substituted NECA; **6**, CGS21680; **7**, BAY 60-6583)

The xanthine moiety of the ligand is commonly oriented as it gives an aromatic stacking interaction with Phe168 and the lipophilic cage made up of Met177, Ile252, Leu249, Ala273, Met270 Ile274, Met174, and Trp246. Moreover, the propargyl moiety at the 1-position of the ligand is bordered by Asn181, Val186, Leu85, and His250. Furthermore, the propyl moiety of the ligand is located inside the pocket formed by Ala59, Val55, Val84, Ile60, Leu87 and Val275, whereas the methyl moiety of the ligand is placed in the pocket formed by Leu167, Gly69, His264, and Leu267.

The final result for istradefylline (compound **9** in Fig. 2) follows the general pattern [45]. As before, the hydrogen bonding and lipophilic interactions are maintained.

The obtained result for the non-xanthine antagonist preladenant [46] (compound **18** in Fig. 2) in complex with the A_{2A} receptor is virtually the same as that of ZM241385, where the bicyclic and tricyclic moieties of these two ligands reside in a similar position. Additionally the two oxygen atoms of the methoxyethoxy moiety of the ligand interact with two water molecules and the methoxy oxygen atom is predicted to be in proximity to Asn154. Furthermore, the amino group at the 4-position of triazole moiety of the ligand constitutes a water-mediated interaction with Ala81.

Besides, Tyr271 is located near the amino group at the 1-position of the piperazine moiety of the ligand at the same time, His264 is placed near the amino group at the 4-position of the piperazine moiety of the ligand which is believed to be critical for binding and contributes to an increase in the affinity of the ligand (Table 1). In addition, the phenyl moiety of the ligand makes favourable hydrophobic interactions with Leu267, Leu167, and Val171. The tricyclic structure of the pyrazolotriazolopyrimidine, the presence of

Table 1 Interactions (in kcal mol^{-1}) between the A_{2A} antagonists and the important residues based on the energy decomposition analysis MM/PBSA

Residue/A_{2A}	ZM241385	MSX-2	Istradefylline	Preladenant	MRS1706	MRE2029F20	PSB-601
Asn253	**−7.6**	**−4.9**	**−5.1**	**−7.2**	−2.1	−1.2	−1.7
Glu169	**−9.3**	−3.0	−3.0	**−10.9**	**−5.2**	**−4.9**	−0.1
Phe168	−4.5	−5.6	**−6.4**	**−8.1**	−5.0	**−9.4**	**−6.2**
Leu249	**−3.8**	**−4.6**	**−4.1**	**−4.0**	−3.3	−2.1	−2.8
Trp246	−0.5	**−1.9**	**−1.2**	−0.7	**−1.6**	−0.9	**−2.5**
Leu85	−1.0	−1.0	**−1.1**	−1.0	**−3.7**	**−1.2**	**−2.3**
His250	−0.5	**−2.0**	**−1.0**	−0.7	**−1.7**	−0.2	**−1.4**
Val84	−0.5	−1.8	**−2.3**	−0.4	**−1.9**	**−2.9**	**−1.9**
Thr88	−0.1	**−0.3**	−0.1	−0.2	**−4.7**	**−0.2**	**−3.3**
His278	−0.0	**−3.2**	**−0.7**	−0.0	**−1.6**	**−0.6**	-0.2
Met177	−1.8	**−2.2**	**−1.9**	**−1.9**	**−1.9**	−1.0	−1.7
Phe255	−0.0	−0.0	−0.0	−0.0	−0.0	−0.0	−0.0
Ile252	**−0.6**	−0.2	−0.2	**−0.5**	−0.1	−0.1	−0.2
Ala63	−0.1	**−0.4**	**−0.6**	−0.1	−0.1	**−1.4**	**−0.2**
Leu269	−0.1	−0.1	−0.1	−0.1	−0.1	−0.0	**−0.2**
His264	**−1.0**	−0.3	−0.3	**−1.4**	**−1.5**	**−1.8**	−0.4
Leu267	**−2.3**	−0.3	**−1.0**	−0.5	**−2.1**	**−1.0**	**−1.5**
Tyr271	**−1.0**	−0.5	**−1.7**	**−1.3**	−0.5	−0.5	**−0.9**
Ala265	−0.1	−0.1	−0.0	−0.1	−0.1	−0.1	−0.0
Ser263	−0.0	−0.0	−0.0	−0.0	−0.0	−0.0	−0.0
Pro266	**−0.1**	−0.0	−0.0	**−0.1**	−0.0	−0.0	**−0.1**
Leu167	−0.6	**−2.0**	−1.7	**−2.8**	−1.9	**−3.9**	**−2.7**
Asp170	−0.2	−0.2	**−0.3**	**−3.8**	−0.2	**−1.9**	−0.2
Ser67	−0.2	**−0.7**	**−1.1**	−0.2	−0.1	**−0.7**	**−3.5**
Ala165	−0.0	−0.0	−0.0	−0.1	−0.0	−0.0	−0.2
Ala81	−0.2	−0.2	−0.5	−0.2	−0.2	**−1.3**	−0.3

The most significant interactions are highlighted in bold in order to emphasize the respective interaction patterns

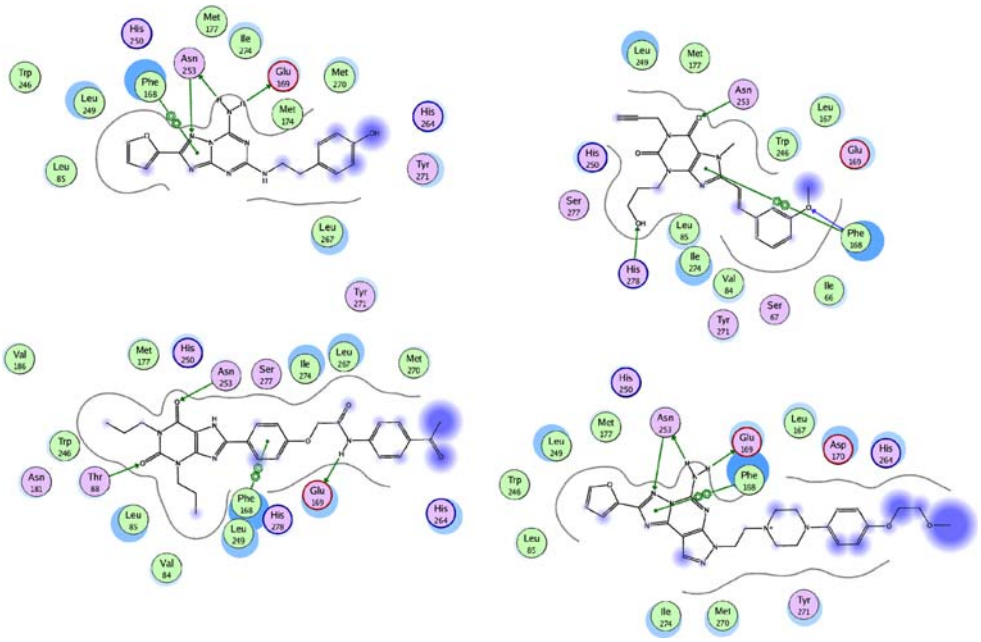

Fig. 4 Predicted binding modes for ZM241385 (*up left*), MSX-2 (*up right*), MRS1706 (*down left*) and Preladenant (*down right*). Shown are hydrogen bonds and aromatic stacking interactions

the furan ring, the exocyclic 5-amino group, and the aryl–alkyl substituent on the nitrogen at the 7-position are probably essential for both affinity and selectivity for the A_{2A} receptor. Also, because of the existence of additional hydrogen bonding and desirable interactions, preladenant has higher affinity towards the A_{2A} adenosine receptor than the other ligands (Fig. 4).

In the most favourable location we found for MRS 1706 [47] (compound **11** in Fig. 2) in the A_{2A} receptor that again the Asn253 side-chain forms a hydrogen bonding interaction with the carbonyl group at the 6-position of the ligand. However, the NH group at the 7-position of the ligand is located far away from Asn253. The amino group at the 9-position of the ligand is involved in a hydrogen bonding interaction with a water molecule.

Additionally, Thr88 forms a hydrogen bonding interaction with the carbonyl group at the 2-position of the ligand and Glu169 forms a hydrogen bonding interaction with the amino group of the phenoxyacetamide moiety of the ligand. The propyl group at the 1-position is located inside the hydrophobic pocket formed by Val186, Phe182, Thr88, Leu85, Gln89, Ile135 and Ile92. Likewise the propyl group at the 3-position is in contact to Ala59, Val55, His278 and Val84. Moreover, the phenylxanthine moiety of the ligand is involved in hydrophobic interactions with Ile66, Ala63, Ile274, Leu249, His250, Ala81, Met177 and Trp246 and stabilized by an aromatic interaction with Phe168. Besides that, the carbonyl oxygen atom of the acetyl group of the ligand forms water-mediated interactions with His264 and Asp170. Furthermore, the acetylphenyl group of the ligand is predicted to be involved in an aromatic stacking interaction with His264 and located inside the pocket formed by Leu167, Met270, Leu267 and Tyr271 (Fig. 4).

The result from our docking study of MRE2029F20 [48] with the A_{2A} receptor (compound **12** in Fig. 2) is that the hydrogen bonding interaction between Asn253 and the carbonyl group at the 6-position of the ligand as well as the hydrogen bonding interaction between the carbonyl group at the 2-position of the ligand and Thr88 is lost due to unfavourable interactions and the steric effect induced by the bulky fragment of the ligand. The carbonyl group of the oxyacetamide moiety of the ligand is hydrogen-bonded to the backbone amino group of Phe168. At the same time, the amino group of the oxyacetamide moiety of the ligand forms a hydrogen bonding interaction with a water molecule. The pyrazolylxanthine moiety of the ligand is located inside the pocket similar to that of the phenylxanthine moiety of MRS1706. In addition, the methylenedioxyphenyl moiety of the ligand is surrounded by Asp170, Glu169, Thr256, Leu167, His264 and Leu267.

The obtained binding mode for PSB-601 [49] (compound **10** in Fig. 2) suggests that the arrangement of the ligand is similar to that of MRS1706. However, the interaction between Asn253 and the carbonyl group at the 6-position and the NH group at the 7-position of the ligand is lost. In addition, the Thr88 side-chain forms a hydrogen bonding interaction with the carbonyl group at the 2-position of the ligand. The lipophilic interaction is maintained and adopted the same cavity in the active site similar to that of MRS1706. The predicted binding rank of MRS1706 and PSB-601 with the A_{2A} receptor is consistent with the experimental results. According to the predicted binding modes of the complexes, the residues in the active site of MRS1706 and PSB-601 give similar contribution for the A_{2A} adenosine receptor. This is reasonable because the active sites of the complexes have similar residues and volume. However, MRS1706 ($K_i = 112$ nM) binds to the active site and has additional interactions. Moreover, Leu85, Thr88, Asn181, and His278 are close to the active site and responsible for increasing affinity but PSB-601 ($K_i = 484$ nM) did not bind so well.

The outcome of the docking analysis of the A_{2A} receptor indicates that all xanthine and nonxanthine type antagonists have similar binding mode patterns and the above results are in a good agreement with the experimental data collected in (Table 2). By combining the docking results from the above discussed antagonists, we were able to extract some residues, which could be essential for different ligands to bind potential A_{2A} antagonists. In particular, Val84, Glu169, His250, Asn253, His278, Phe182, Glu151 and Ile274 are crucial for the antagonist recognition, while Val84, Phe182, His278, Ser277 and His251 are also involved in agonist binding. Moreover, the hydrophobic interaction domains located at the binding pocket are supposed to importantly contribute to the binding affinity of A_{2A} antagonists. In summary, it is reasonable to suggest that Ile80, Leu249, Ile252, Met270, Ala59, Leu167, Asn154, His264, Leu267, and Tyr271 could be responsible for the selectivity of adenosine A_{2A} receptor ligands.

Docking of agonists (NECA, BAY60-6583 and CGS21680) into the A_{2A} receptor in order to study performance of receptor structure with agonists

The obtained result for NECA [50] an analogue of the native agonist (compound **3** in Fig. 3) is that the amino group at the 6-position of NECA is involved in a hydrogen bonding interaction with the carbonyl oxygen atom of Asn253, and Glu169 is located at a distance of 5.69 Å from the amino group at the 6-position of NECA. In addition, the amino group at the 7-position of NECA forms a hydrogen bond with a water molecule.

Additionally, the 3′-hydroxyl group of the ligand forms water-mediated interactions with Ala59 and Ile80, while the 2′-hydroxyl group of NECA constitutes water-mediated interactions with Ile80 and Ala81. At the same time, the

Table 2 Effects of mutation of single amino acids in adenosine A_{2A} and A_{2B} receptors on antagonist and agonist binding and/or function

A_{2A}	Effect	A_{2B}	Effect
$E13^{1.39}$	Q: slight reduction of Ag but not Ant affinity [62]	$V11^{1.36}$	NC for Ag [63]
$V84^{3.32}$	A/D: loss of Ag & Ant radioligand binding, L: slight increase in Ag and decrease in Ant affinity [64]	$A12^{1.37}$	NC for Ag [63]
$T88^{3.36}$	A/S/R/E: substantial decrease in Ag but not Ant activity [65]	$N36^{IL1}$	NC for Ag [66]
$Q89^{3.37}$	A: slight increase in Ag and Ant activity, D: slight increase in Ag but not Ant affinity, N/S/L: marginal changes in ligand binding, H/R: Ant binding affected [65]	$T42^{2.39}$	Decrease in Ag activity (4.9-fold) [66]
$S90^{3.38}$	A: marginal changes in ligand binding [65]	$V54^{2.51}$	Decrease in Ag activity (6.3-fold) [66]
$S91^{3.39}$	A: marginal changes in ligand binding [65]	$L58^{2.55}$	NC in Ag [63]
$E151^{EL-2}$	A/Q/D: loss of Ag and Ant binding, ~1,000-fold decrease in Ag potency [67]	$F59^{2.56}$	No specific binding and no cAMP production [63]
$E169^{EL-2}$	A: loss of Ag and Ant binding, ~1,000-fold decrease in Ag potency, Q: gain in Ag affinity [67]	$F84^{3.31}$	Decrease in Ag activity (3.1- to 6.5-fold) [66]
$D170^{EL-2}$	K: NC in ligand binding [67]	$S91^{3.38}$	NC in Ag [66]
$P173^{EL-2}$	R: NC in ligand binding [67]	$N273^{7.36}$	NC for Ant, NC for Ag except for CGS21680 (decrease of 3.2-fold) and other 2-substituted adenosines [63]
$F180^{5.41}$	A: minor changes in ligand binding [68]		
$N181^{5.42}$	S: modest reduction of Ag binding [68]		
$F182^{5.43}$	A: loss of Ag and Ant binding, Y, W: modest reduction of Ag binding [68]		
$H250^{6.52}$	A: loss of Ag and Ant binding, no Ag activity in functional assays, F, Y: modest reduction of Ag binding; no effect on Ant binding, N: slight increase in Ag affinity, minor changes in Ant affinity [64, 68]		
$N253^{6.55}$	A: loss of Ag and Ant radioligand binding [68]		
$C254^{6.56}$	A: minor changes in ligand binding [68]		
$F257^{6.59}$	A: loss of Ag and Ant radioligand binding [68]		
$C262^{EL-3}$	G: NC in radioligand binding [67]		
$I274^{7.39}$	A: loss of Ag and Ant binding, 30-fold decrease in Ag potency [68]		
$S277^{7.42}$	A: substantial decrease in only Ag activity and potency, T/C/N/E: marginal changes in binding [64, 67]		
$H278^{7.43}$	A: loss of Ag and Ant binding; 300-fold decrease in Ag potency, Y: modest reduction of Ag binding; NC on Ant binding, D/E: marginal changes in binding [68, 69]		
$S281^{7.46}$	A: loss of Ag and Ant radioligand binding; no Ag activity in functional assay, T: enhanced activity for Ag, N: marginal changes in ligand binding [68, 69]		

Ag Agonist, *Ant* antagonist, *NC* no change

carbonyl group at the 5′-position of NECA forms a hydrogen bonding interaction with a water molecule and Ser277 is located at a distance of 5.63 Å from the carbonyl group at the 5′-position of NECA. Moreover, His278 is located at a distance of 4.65 Å from the 5′-amino group of NECA. The adenine moiety of NECA is stabilized by an aromatic stacking interaction with Phe168 and hydrophobic interactions with Trp246, Met270, Met174, Met177, Leu85, Leu249, His250, Ile252, Ala273, and Ile274. Furthermore, the ribose moiety of NECA is surrounded by Ala81, Ile66, Val84, Ala63, and Thr88.

The adenosine A_{2A} selective agonists usually contain a bulky substituent in the 2-position of the adenine ring of NECA. Also, some analogs of NECA substituted in the 2-position of the adenine ring by an alkyl group as well as an aromatic or heteroaromatic ring showed high potency at the A_{2A} receptor. For example, CGS21680 was shown to be a selective agonist for the A_{2A} adenosine receptor. The proposed binding mode of CGS21680 [51], a NECA-derivative (compound **6** in Fig. 3) in A_{2A} receptor is much the same as that of NECA. In addition the phenyl moiety of the ligand shows aromatic stacking interaction with

Trp246, it also interacts with His250 and shows aliphatic hydrophobic interactions with Phe182, Phe242, Val186, Leu85, Thr88, Val86, Leu87, Cys185, and Ile92, a pocket that contributes to an increase in the affinity and selectivity of the ligand. The hydroxyl group of the carboxylate moiety of the ligand is involved in a hydrogen bonding interaction with Asn181. In addition, the side chains of Gln89, Thr138, Tyr176, Ser132, and the backbone carbonyl group of Phe180, Ile135 are observed in proximity to the hydroxyl group of the carboxylate moiety of the ligand.

Our study has confirmed that the interaction with Asn253 is crucial, which is suggested by mutagenesis studies to be of great importance for this receptor subtype. Moreover, it was assumed that the presence of His250 is required in the binding pocket but a hydrogen bonding is not necessary. The docking of CGS21680 shows that the selectivity of this compound could be due to the presence of Glu169, Ile80, Leu249, Ile252, Ser132, Val172, and Ala59 which are able to interact with the ligand. In addition, the results show that the A_{2A} selectivity is not mainly influenced by a different hydrogen bonding network between ligand and receptor but also by lipophilic interactions. These findings may provide a possible explanation for the higher selectivity of this agonist for the A_{2A} adenosine receptor in comparison to the A_{2B} receptor.

Initially, we tried to place the A_{2B} agonist BAY60-6583 [52] into the putative A_{2A} binding site similarly to its placement in the A_{2B} receptor. However, undesirable steric effects, resulting from the absence of sufficient free space to accommodate the ligand, were observed. The obtained result of molecular docking of BAY60-6583, a non-adenosine agonist, suggests that the amino group at the 6-position of BAY 60-6583 (compound **7** in Fig. 3) forms hydrogen bonding interactions with the amide oxygen atom of Asn253 and the backbone carbonyl group of Met177, additionally Val178 and Phe182 are closer to this moiety.

The side-chain of Asn181 and the backbone carbonyl group of Leu85 form hydrogen bonding interactions with the amino group of the sulfanylacetamide moiety of the ligand, and the side chains of Ile92 and Ile135 are located near the amino group of the sulfanylacetamide moiety of the ligand. Furthermore, Gln89 forms a water mediated interaction with the carbonyl group of the sulfanylacetamide moiety of the ligand. Besides, the cyano group at the 3-position of the ligand is located at a distance of 3.09 Å from Thr88. The phenylpyridine moiety is located inside the hydrophobic pocket formed by Val84, Leu85, Met174, Phe168, Met177, His250, Leu249, Trp246, and Val186, while the cyclopropyl residue is surrounded by Ile66, Ala63, Ala59, Phe62, Ala81, Ile80, Cys82, Ile274, and His278.

The results from our molecular docking of the agonists showed that the results are in accordance with experimental data and Val84, Thr88, Gln89, Glu169, Asn181, Phe182, His250, Asn253, Ile274, Ser277, and His278 are essential for A_{2A} agonist docking and the selectivity of the A_{2A} receptor could be due to the presence of Glu169, Ile80, Leu249, Ile252, Ser132, Val172, and Ala59.

Probing of the adenosine A_{2B} models by docking of selected antagonists (**theophylline**, ZM241385, MRS1706, and PSB-601) and selection of the most suitable model for further studies

The obtained binding mode for the most simple, known antagonist theophylline [53] (compound **1** in Fig. 2) in the A_{2B}-I model suggests that the Asn254 side-chain forms hydrogen bonding interactions with the carbonyl group at the 6-position and the NH group at the 7-position of the xanthine ring. In addition, the Gln90 side-chain fixes the ligand by another hydrogen bonding interaction to the carbonyl oxygen atom at the 2-position of the xanthine ring and the amino group at the 9-position of the xanthine ring interacts with a water molecule.

Furthermore, the methyl group at the 1-position is stabilized by lipophilic interactions with Val191, and Phe187, while the methyl group at the 3-position can interact with Thr89, Ile136, and Leu86. The xanthine moiety of the ligand forms an aromatic stacking interaction with Phe173 and lies inside the pocket formed by Leu172, Val183, His250, and Trp247. The binding mode in the A_{2B}-II model is generally the same as in the A_{2B}-I model, except that Asn186 forms a water mediated interaction with the carbonyl group at the 6-position of the ligand. However, in the A_{2B}-III model the carbonyl oxygen atom at the 2-position of the xanthine ring interacts with a water molecule (Fig. 5).

The obtained binding mode of ZM241385 [43] (compound **13** in Fig. 2) with the A_{2B}-III model allowed us to propose that the bicyclic triazolotriazine core of ZM241385 is stabilized by an aromatic stacking interaction with Phe173, aliphatic hydrophobic interactions with Val250, Met272, Met179, Val253, Met182, and Ile276, and hydrogen bonding interactions with Asn254 and Glu174 (conjugated hydrogen bonding from Thr257 through Glu174 and Asn254 to the exocyclic amino group), which interacts with the exocyclic amino group.

Furthermore, Asn254 interacts with the furan oxygen atom and the amino group at the 1-position of the triazolotriazine moiety of the ligand. At the same time, the furan oxygen atom is in proximity to the backbone amino group of Asn186. In addition, the furan ring is stabilized by hydrophobic interactions with Leu86, His251, and Val85, and the furan ring is approximately 4.3 Å away from the highly conserved Trp247. Moreover, the phenolic hydroxyl group forms a hydrogen bonding with the backbone

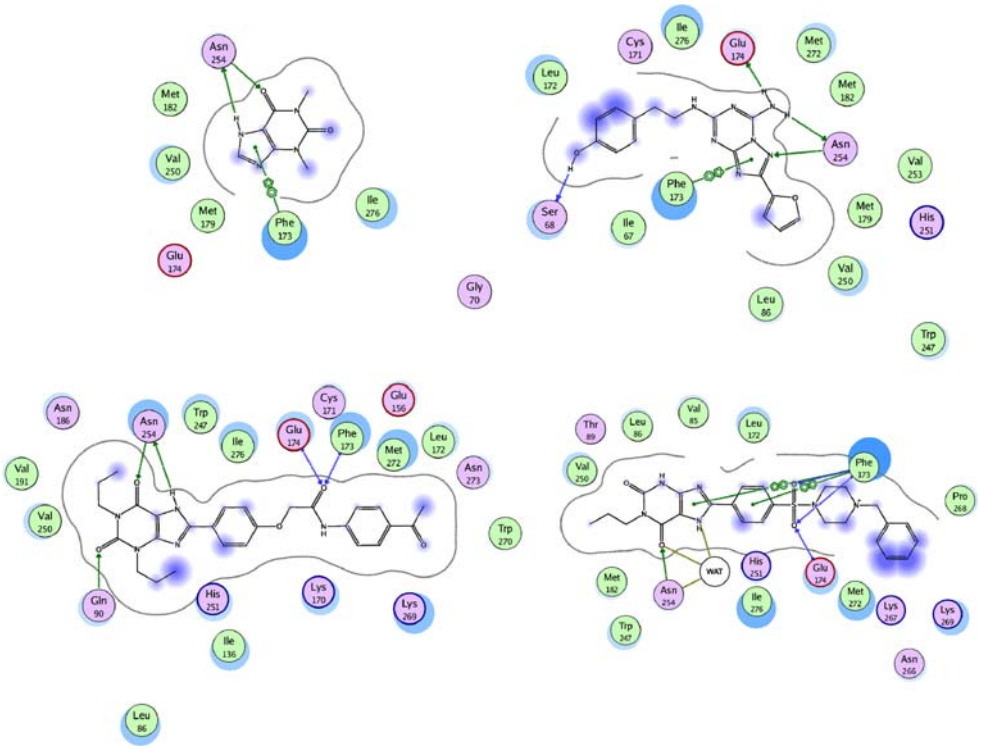

Fig. 5 Predicted binding modes for theophylline in model A_{2B}-I (*top left*), ZM241385 in model A_{2B}-III (*top right*), MRS1706 in model A_{2B}-II (*bottom left*) and PSB-601 in model A_{2B}-I II (*bottom right*). Shown are hydrogen bonds and aromatic stacking interactions

carbonyl group of Ser68 and the phenyl ring forms hydrophobic interactions with Ile67, Gly70, and Leu172. Furthermore, Lys269 is located near the phenol moiety of the ligand (Fig. 5).

The most favourable position of the phenyl ring of ZM241385 was surrounded by Leu267, Tyr271, and His264 of the A_{2A} receptor, however, this most favourable arrangement of the phenyl ring of ZM241385 inside the A_{2A} receptor has two serious drawbacks in comparison to the binding mode obtained for the A_{2B} receptor. Firstly, in the A_{2B} receptor the phenyl ring of the ligand was located near Lys269, which resulted in unfavourable interactions. Second, because of the large distance Lys269 was unable to form the very important interaction with the phenyl ring of the ligand. These results might provide an explanation for the considerable difference between the K_i values of ZM241385 determined for the A_{2A} (0.8 nM) and A_{2B} (50 nM) and Leu267, Tyr271, His264, Leu249, and Ile252 could be responsible for increasing the affinity towards the adenosine A_{2A} receptor. The binding modes for the A_{2B}-I and A_{2B}-II models are similar to that of A_{2B}-III model however, in the A_{2B}-II model His280 is directly involved in a hydrogen bonding interaction with the phenolic hydroxyl group of the ligand.

The placement of MRS 1706 [47] (compound **11** in Fig. 2) in the model A_{2B}-II is that the Asn254 side-chain forms hydrogen bonding interactions to the carbonyl group at the 6-position and the NH group at the 7-position of the ligand. In addition, His251 forms a hydrogen bond to the carbonyl group at the 6-position of the ligand and the Gln90 side-chain constitutes a hydrogen bonding interaction with the carbonyl oxygen atom at the 2-position of the ligand. Besides that the backbone amino group of Phe173 forms a hydrogen bond with the carbonyl oxygen atom of the phenoxy acetamide moiety of the ligand. The propyl group at the 1-position is located inside the hydrophobic pocket formed by Val183, Phe187, Val191, and Cys190. Likewise the propyl group at the 3-position is in contact to Thr89, Leu86, Ile136, and Pro140. Moreover, the xanthinephenyl moiety of the ligand is involved in hydrophobic interactions with Phe173, Val250, Met272, Ile276, Val253, and Trp247.

The phenyl ring of the phenoxy acetamide moiety of the ligand resides in the hydrophobic pocket formed by Leu172 Trp270, and the lipophobic part of Lys269 and makes favourable cation–π interactions with Lys170 and Lys267. The obtained position of MRS-1706 in the A_{2B}-I and A_{2B}-III model is similar to that in the previous one, except that in the A_{2B}-I model Glu14, Asn186, and His280 are directly involved in an interaction (Fig. 5).

The obtained binding mode for PSB-601 [49] (compound **10** in Fig. 2) in the model A_{2B}-III suggests that the Asn254 side-chain forms hydrogen bonding interactions with the carbonyl group at the 6-position and the NH group at the 7-position of the ligand. Besides that, the backbones of Glu174, Phe173 and a water molecule form hydrogen

Table 3 Interactions (in kcal mol^{-1}) between the A_{2B} antagonists and the important residues based on the energy decomposition analysis MM/PBSA

Residue/A_{2B}	ZM241385	MSX-2	Istradefylline	Preladenant	MRS1706	MRE2029F20	PSB-601
Asn254	**−6.9**	−2.3	**−4.6**	**−6.1**	−3.8	**−4.7**	−4.2
Glu174	**−8.2**	−1.2	−0.7	**−4.4**	**−4.9**	**−5.2**	−3.2
Phe173	−5.7	−6.0	−6.4	**−6.6**	**−6.6**	**−7.7**	**−7.7**
Val250	−2.5	**−2.8**	**−2.7**	−2.3	**−3.0**	**−3.1**	−2.4
Trp247	−0.7	−0.9	**−1.5**	−0.8	**−1.9**	**−1.8**	**−1.9**
Leu86	−1.0	**−1.4**	**−1.5**	−1.0	**−1.3**	**−1.4**	−1.2
His251	−0.7	−0.7	**−0.9**	−0.5	**−1.8**	**−1.6**	**−1.2**
Val85	−0.3	**−4.4**	**−2.0**	−0.6	**−1.4**	**−1.7**	−1.1
Thr89	−0.2	**−0.5**	−0.2	−0.3	**−0.8**	**−0.6**	**−0.6**
His280	−0.0	**−2.1**	**−0.8**	−0.1	**−1.5**	**−0.8**	−0.2
Met182	−1.7	**−2.1**	**−2.5**	−1.8	**−1.9**	**−1.9**	**−2.1**
Val256	−0.0	−0.0	−0.0	−0.0	−0.0	−0.0	**−0.1**
Val253	**−0.7**	**−0.4**	−0.3	**−0.5**	−0.2	−0.2	**−0.5**
Ala64	−0.1	**−1.3**	**−0.5**	−0.1	**−0.8**	**−0.5**	−0.2
Ala271	−0.1	−0.1	−0.1	−0.1	−0.1	−0.0	**−0.3**
Asn266	−0.0	−0.1	−0.1	**−0.6**	**−0.2**	**−0.2**	**−2.0**
Lys269	−0.2	**−0.4**	**−0.4**	−0.2	−0.1	−0.1	**−2.1**
Asn273	−0.1	−0.1	−0.2	−0.1	−0.1	−0.2	−0.2
Lys267	−0.1	**−0.3**	−0.1	−0.1	−0.1	−0.1	**−0.4**
Lys265	−0.0	**−0.2**	−0.0	−0.1	−0.0	−0.0	**−0.2**
Pro268	−0.0	−0.0	−0.0	−0.1	−0.0	−0.0	−1.0
Leu172	**−2.8**	−1.9	−2.1	**−2.8**	**−4.5**	**−4.5**	**−3.4**
Asn175	−0.1	−0.1	−0.1	**−2.0**	**−4.3**	**−2.5**	−0.2
Ser68	**−1.7**	**−0.8**	**−1.3**	−0.1	**−0.4**	−0.1	−0.3
Lys170	−0.2	**−0.3**	−0.1	−0.1	−0.1	−0.1	−0.1
Ala82	−0.1	**−1.6**	**−0.4**	−0.2	−0.2	**−0.6**	−0.2

The most significant interactions are highlighted in bold in order to emphasize the respective interaction patterns

bonding interactions with the sulfonyl group of the ligand. Furthermore, the backbone amino group of Asn175 is in proximity to the sulfonyl group of the ligand (Table 3).

In addition, the amino group at the 9-position of the ligand is involved in a hydrogen bonding interaction with a water molecule. Additionally, the propyl group at the 1-position of the ligand is located inside the hydrophobic pocket formed by Leu86, Val85, Thr89, His251, and Val191. The phenylxanthine moiety of the ligand is stabilized by an aromatic stacking interaction with Phe173 and located inside the pocket formed by Ala64, Ile67, Met179, Ile276, His280, Met182, Val250, and Trp247. Moreover, the benzylpiperazine moiety of the ligand is surrounded by Leu172, Lys265, Pro268, Met272, and Lys269. As before, the binding modes for the A_{2B}-I and A_{2B}-II models are similar to that of the A_{2B}-III model, however, in the A_{2B}-I model Leu81, Lys170, Asn186 and His280 are directly involved in interactions (Fig. 5).

Both investigated models, A_{2B}-I and A_{2B}-II yielded concordantly the same binding modes, which overlaps significantly with the binding site for the adenosine A_{2A} receptor. However, A_{2B}-III has a different binding mode where the ligands bind in an extended conformation and its orientation is almost perpendicular to the membrane plane and co-linear with transmembrane helix VII. As a next step, the complex properties were not only investigated with respect to the sterical and electronic aspects of the binding modes, but in addition the estimated binding affinities were taken into account. As shown in (Table 4) the calculated free binding energies ΔG for the A_{2B}-I, A_{2B}-II and A_{2B}-III models are similar. In summary, all models perform equally well, quantitatively, i.e. in terms of relative binding affinities, the results were equivalent. However, qualitatively, i.e. in terms of predicted binding modes they were different. For further studies we chose model A_{2B}-III which is the one with the highest sequence identity (56%), the lowest RMSD value (relative to the adenosine A_{2A} receptor), the most favourable gap ratio, and the obtained results are in accordance with experimental data where His280 might not be important for ligand binding

Table 4 The calculated ΔG free energy of binding and binding affinities for all models

Ligand	Calculated ΔG (A_{2B}-I) (kcal mol^{-1})	Calculated ΔG (A_{2B}-II) (kcal mol^{-1})	Calculated ΔG (A_{2B}-III) (kcal mol^{-1})
Theophylline [53]	−48.0 ± 0.6	−45.0 ± 1.2	−48.1 ± 1.0
ZM241385 [43]	−80.0 ± 3.0	−80.0 ± 1.0	−86.1 ± 4.0
MRS1706 [47]	−114.0 ± 3.3	−99.1 ± 4.1	−115.0 ± 3.0
PSB-601 [49]	−100.0 ± 2.0	−94.0 ± 1.0	−106.0 ± 4.0
RMSD (Å)	3.25	3.29	0.8

but for maintaining the global receptor architecture (S. Hinz, A. Schiedel, C. E. Müller, unpublished results). In order to validate this model further, we subsequently compared the binding modes and affinities of a larger set of compounds with experimental data.

In order to cover a wider range of ligands, we studied some smaller and more weakly binding ligands as well. The obtained results for 1,3-dipropylxanthine, 1-propylxanthine, 1-butylxanthine, and 1-allylxanthine [53] (compounds **2**, **3**, **4** and **5** in Fig. 2) suggest that the Asn254 side-chain consistently forms hydrogen bonding interactions with the carbonyl oxygen atom at the 6-position and the NH group at the 7-position of the xanthine ring. Furthermore, a water molecule forms a hydrogen bonding interaction with the carbonyl oxygen atom at the 2-position of the xanthine ring. The substituted group at the 1-position is located inside the binding pocket formed by Leu86, Thr89, and Val85, while the substituted group at the 3-position is involved in ligand binding via interaction with Ile67, Ala82, Ile276, and Ala64. The xanthine moiety is stabilized by an aromatic stacking interaction with Phe173 and located inside the pocket formed by Met182, His251, Trp247, Val250, Val253, Met272, and Met179.

According to the computed binding mode for 1-propyl-8-cyclopentylxanthine [53] (compound **6** in Fig. 2) the Asn254 side-chain forms two hydrogen bonding interactions, one to the carbonyl oxygen atom at the 6-position and the other one to the NH group at the 7-position of the xanthine ring. In addition, a water molecule stabilizes the ligand's position by a hydrogen-bonding interaction with the amino group at the 3-position of the xanthine ring. The propyl group at the 1-position is located inside the binding pocket formed by Val85, Leu86, Val191, and Thr89. The xanthine moiety is stabilized by an aromatic interaction with Phe173 and lies inside the pocket formed by Ala82, trp247, Val250, His251, Met179, and Met182. Furthermore, the cyclopentyl ring is surrounded by Val253, Ala275, Ile276, and Met272.

The proposed binding mode for PBS-1115 [54] (compound **7** in Fig. 2) is much the same to that of 1-propyl-8-cyclopentylxanthine. Additionally, the sulfonate function of the ligand is stabilized by interactions with the side chains of Asn266, Thr257, and the backbone amino group of Lys267. The results are in agreement with mutagenesis data for the closely related human adenosine A_{2A} receptor subtype (Table 2) and are consistent with structure–activity relationships (SARs) of a series of sulfonamide derivatives of PSB-1115 bearing a large variety of substituents [49].

The result from our docking study with MRE2029F20 [48] (compound **12** in Fig. 2) was that the Asn254 side-chain directly interacts with the xanthine moiety of the ligand as before. In addition, a water molecule is involved in a hydrogen bonding interaction with the amino group at the 9-position of the ligand. The propyl group at the 1-position is stabilized by lipophilic interactions to Leu86, Val191, Met182, and Thr89, while the propyl group at the 3-position is neighbouring the residues Ala60, Val85, Ala82, His280, and Ala64. The carbonyl group of the oxyacetamide moiety of the ligand is hydrogen-bonded to the backbone amino groups of Glu174 and Phe173. At the same time, the amino group of the oxyacetamide moiety of the ligand forms a hydrogen bonding with a water molecule. The pyrazolylxanthine moiety of the ligand is located inside the pocket formed by Ile67, Met179, Trp247, Val250, Ile276, His251, and Met272 and stabilized by an aromatic interaction with Phe173. In addition, the methylenedioxyphenyl moiety of the ligand is surrounded by lipophilic groups of Leu172 and by polar groups of Asn175, Thr257, and Gln263.

The molecular docking performed for the 4′-furan-2-yl-*N*-pyridin-3-yl-4,5′-bipyrimidin-2′-amines as potent and selective adenosine A_{2B} receptor antagonist [55] (compounds **15**, **16**, and **17** in Fig. 2) suggests that Asn254 is involved in an interaction with the furan oxygen atom and the amino group at the 2′-position of the ligand and the furan moiety of the ligand is located in the pocket formed by Thr89, His251, Val191, and Leu86. Additionally, the nitrogen atom of the pyridine moiety of the ligand is stabilized by a hydrogen bonding interaction with Thr257 and hydrophobic interactions with Val253 and Met272. A water molecule constitutes an interaction between the nitrogen atom at the 1′-position of the ligand. Furthermore, the nitrogen atom at the 1-position of the pyrimidine moiety of the ligand is potentially kept in its position by a hydrogen bond to the protonated nitrogen atom of His280. In addition, the bipyrimidine moiety of the ligand is located in the hydrophobic pocket formed by Ala60, Ala64, Trp247, Val250, Met182, Met179, Ala275, Vla85, Phe173, Ala82,

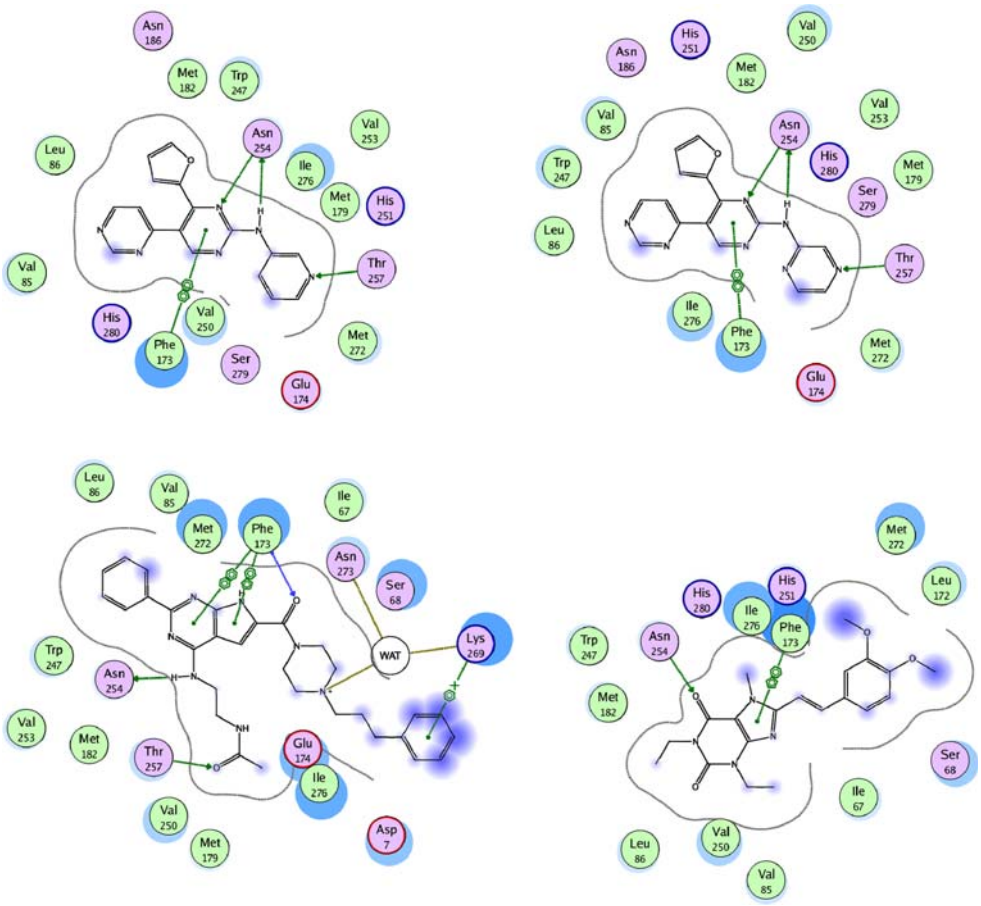

Fig. 6 Predicted binding modes for ligand 15 (*top left*), ligand 16 (*top right*), OSIP339391 (*bottom left*) and istradefylline (*bottom right*). Showing hydrogen bonds, aromatic stacking and aromatic-cation interactions

and Ile67. The obtained binding modes are comparable for all three members of this type of antagonists (Fig. 6).

The obtained binding mode for OSIP339391 [56] (compound **14** in Fig. 2) shows that the amino group attached to the heterocycle is involved in a hydrogen bonding interaction with Asn254 and the carbonyl group of the acetamide moiety of the ligand is hydrogen bonded to Thr257, and Asn266 is located in proximity to the carbonyl group of the acetamide moiety of the ligand. Furthermore, the phenyl moiety of the ligand is stabilized by an aromatic interaction with Trp247 and involved in hydrophobic interactions with Leu86, His251, Met182, Val85, and Thr89 however, the pyrrolopyrimidine moiety of the ligand is stabilized by an aromatic interaction with Phe173 and located inside the pocket formed by Val253, Ala275, Met272, Val250, Ile67, Ala64, Ala82, and Ile276. In addition, the methyl moiety of the ligand is placed in the cage formed by Met179 and Thr257. The piperazinylpropylphenyl moiety of the ligand is occupied by a hydrophobic residue such as Leu172. Additionally, the cationic side chain of Lys269 is involved in cation–π interaction with the propylphenyl moiety of the ligand. In particular, this interaction could be suggested to provide significant stability at the solvent-exposed surface of a protein (Fig. 6).

The obtained binding mode of MSX-2 [44] and Istradefylline [45] (compounds **8** and **9** in Fig. 2) into the A_{2B} receptor is similar to that of the A_{2A} receptor where the corresponding residues show the same hydrogen bonding and hydrophobic interactions. In the adenosine A_{2A} receptor the styryl moiety of the ligands are anchored by an aromatic stacking interaction with Tyr271 and hydrophobic interactions with Leu267, and His264. However, the corresponding residues Asn273, Lys269, and Asn266 of the A_{2B} receptor are located within 7 Å from the styryl moiety of the ligand thus unable to connect to this moiety of the ligands (Fig. 6).

The obtained result from molecular docking of preladenant [46] (compound **18** in Fig. 2) with the A_{2B} receptor is comparable to that of the A_{2A} receptor, while the corresponding residues Glu174, Asn273, Lys269, and Asn266 in the case of the A_{2B} subtype, are far away, thus avoiding any favourable interactions.

The results of the docking analysis of the antagonists of the adenosine A_{2B} receptor display a common binding mode for the xanthine and nonxanthine derivatives which is very similar to that of the binding mode of the adenosine A_{2A} receptor. In addition, considering the close relationship of the A_{2A} and A_{2B} adenosine receptor subtypes, the results may be correlated to the mutagenesis data published

Table 5 K_i values from experimental measurements, absolute free binding energies calculated from K_i values, and computed values of ΔG (kcal mol^{-1}) for all antagonist ligands tested in the present study

	Ligand	Experimental K_i value (nM)	Experimental ΔG (kcal/mol)	ΔE_{ELE}	ΔE_{VDW}	Calculated ΔG (kcal/mol)
1	Theophylline [53]	9,070	−6.8 ± 0.1	−26.3 ± 2.0	−21.8 ± 1.6	−48.0 ± 1.0
2	1,3-Dipropylxanthine [53]	1,110	−8.00 ± 0.2	23.4 ± 0.9	−30.7 ± 0.5	−54.0 ± 0.4
3	1-Propylxanthine [53]	360	−8.6 ± 0.1	−30.6 ± 0.7	−24.4 ± 0.8	−54.9 ± 1.1
4	1-Butylxanthine [53]	421	−8.6 ± 0.1	−33.7 ± 1.1	−25.3 ± 1.0	−59.0 ± 0.5
5	1-Allylxanthine [53]	461	−8.5 ± n.a.	−27.5 ± 2.0	−24.3 ± 1.6	−51.8 ± 1.7
6	1-Propyl-8-cyclopentylxanthine [53]	34.4	−10.0 ± 0.2	−31.7 ± 1.7	−35.9 ± 1.1	−67.6 ± 1.1
7	PSB-1115 [54]	53.4	−9.8 ± 0.2	−31.3 ± 4.6	−41.4 ± 1.7	−72.7 ± 4.2
8	MRS 1706 [47]	1.39	−11.9 ± n.a.	−47.9 ± 3.1	−66.8 ± 2.1	−114.7 ± 2.8
9	MRE2029F20 [48]	5.5	−11.1 ± n.a.	−39.1 ± 2.5	−61.7 ± 2.6	−100.8 ± 2.8
10	PSB-601 [49]	3.6	−11.3 ± 0.1	−50.8 ± 3.4	−55.1 ± 1.9	−105.9 ± 3.5
11	2-aminopyrimidine derivative [55]	17	−10.4 ± 0.2	−29.6 ± 1.8	−41.9 ± 1.3	−71.4 ± 0.7
12	2-aminopyrimidine derivative [55]	116	−9.3 ± 0.1	−26.2 ± 0.8	−40.7 ± 0.7	−66.9 ± 1.3
13	2-aminopyrimidine derivative [55]	119	−9.3 ± 0.2	−18.8 ± 1.5	−46.8 ± 1.5	−65.6 ± 1.8
14	Osip339391 [56]	0.5	−12.5 ± 0.1	−53.0 ± 1.4	−61.6 ± 2.7	−114.7 ± 3.4
15	ZM241385 [43]	5.8	−11.0 ± 1.3	−43.9 ± 3.2	−42.1 ± 1.5	−86.1 ± 3.6
16	MSX-2 [44]	10	−10.8 ± n.a	−32.7 ± 2.3	−50.7 ± 1.2	−83.4 ± 1.2

for the much better characterized A_{2A} subtype (Table 2), which in fact confirms the relevance of the identified interaction partners. Moreover, the structural findings are accompanied by energetic aspects. In Table 5 the observed binding energies ΔG for each complex are listed. The experimentally measured values ranged from −6.8 to −12.5 kcal mol^{-1}. As shown in Fig. 7, the computed values reflect the overall trend, but overestimate the ΔG-values by a factor of five (due to the chosen prefactors as mentioned in the "Materials and methods" section).

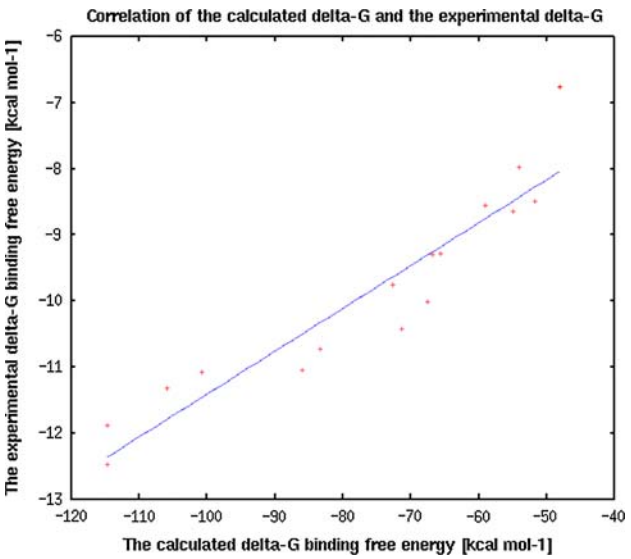

Fig. 7 Correlation of experimental binding free energies ΔG and calculated ΔG values

Docking of agonists

The resulting binding mode of the native agonist adenosine [57] (compound **1** in Fig. 3) implies that the amino group at the 6-position of adenosine forms a hydrogen bonding interaction with the carbonyl oxygen atom of Asn254 (conserved among all adenosine receptor subtypes). Likewise, the 3′-hydroxyl group of the ligand is involved in a water-mediated interaction with Ala60 and located at a distance of 3.69 Å from His280. Additionally, the 2′-hydroxyl group of adenosine constitutes a water-mediated interaction with the backbone carbonyl group of Leu81. The 5′-hydroxyl group might form a hydrogen bonding interaction with Ser279 (located at a distance of 3.3 Å). The adenine moiety is located in the hydrophobic pocket formed by Met179, Met182, Val253, Val250, His251, Ile276, and Trp247 and stabilized by an aromatic stacking interaction with Phe173. Also, the ribose moiety is surrounded by Ala60, Ala64, Ile67, Ala82, Val85, Leu86, and Ile61.

The obtained result for the binding mode of 2-chloroadenosine [58] (CADO, compound **2** in Fig. 3) is similar to that of the above-mentioned adenosine.

The result obtained from our molecular docking study of NECA [50] (compound **3** in Fig. 3) is similar to that of adenosine; additionally, the 2′-hydroxyl group of NECA interacts with the backbone carbonyl oxygen atom of Ala82 (Fig. 8). As shown in Table 6, the calculated free energy of binding ΔG for the A_{2A} crystal structure is much higher than for the A_{2B} model and the electrostatic interactions appeared to be mainly responsible for affinity.

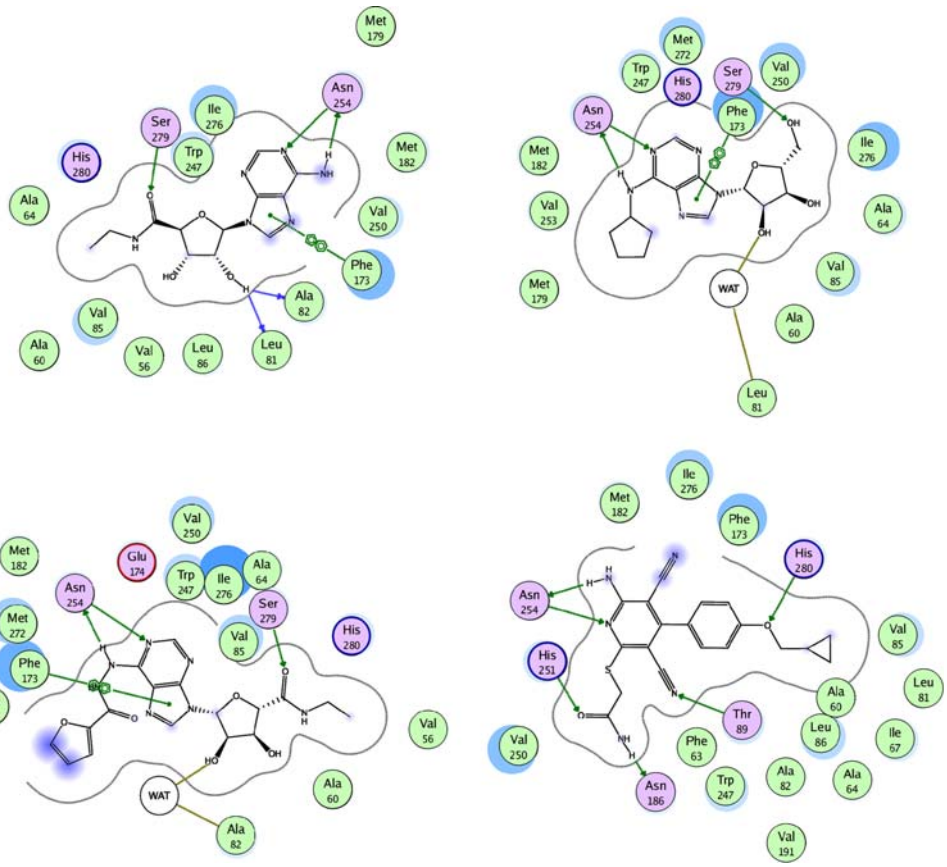

Fig. 8 Predicted binding modes for NECA (*top left*), CPA (*top right*), NECA derivative (*bottom left*) and BAY 60-6583 (*bottom right*). Showing hydrogen bonds and aromatic stacking interactions

Table 6 The calculated ΔG free energy of binding and binding affinities for both the A_{2A} crystal receptor and A_{2B} model

Agonist	Calculated ΔG (A_{2A}) (kcal mol^{-1})	Calculated ΔG (A_{2B}) (kcal mol^{-1})
NECA	−94.92 (ELE = −59.86, VDW = −35.07)	−79.25 (ELE = −39.55, VDW = −39.71)

The higher affinity of NECA towards the adenosine A_{2A} as compared to the A_{2B} receptor most likely can be explained by the following points. Firstly, molecular docking of the A_{2A} and A_{2B} adenosine receptors has detected that the amino group at the 6-position of NECA was hydrogen bonded to $Asn^{6.55}$ conserved among all adenosine receptor subtypes. In the A_{2A} adenosine receptor, Glu169 is located at a distance of 5.20 Å from the amino group at the 6-position of NECA (it could be involved in interaction), while in the A_{2B} model the corresponding Glu174 is located at a distance of 6.6 Å from the amino group at the 6-position of NECA. In addition, the 3′-hydroxyl group of the ligand forms water-mediated interactions with Ala59 and Ile80 and the amino group at the 7-position of the NECA forms a hydrogen bonding with a water molecule. These interactions were not observed for the A_{2B} model.

Secondly, The A_{2A} adenosine receptor has a larger volume of the hydrophobic pocket than the A_{2B} receptor. The size of this hydrophobic pocket of the A_{2A} receptor is large enough to accommodate the ligand which could contribute to increase of the A_{2A} affinity. However, in the A_{2B} receptor, the size of the pocket has a higher degree of conformational flexibility, decreasing the relative stability of the complex.

Thirdly, on the other hand, the A_{2B} receptor agonist was located slightly deeper inside the receptor than the A_{2A} adenosine receptor. These particular features of the A_{2A} adenosine receptor combined with the obtained binding mode allow us to propose an explanation of the high affinity of NECA at this subtype in comparison to the A_{2B} adenosine receptor subtype.

N^6-Cyclopentyladenosine (CPA, compound **4**, Fig. 3) is an agonist, which in contrast to the previous ones, carries a bulky substituent at its 6-position. The predicted binding mode for CPA [58] indicates that the cyclopentyl moiety at the 6-position of the ligand is located inside a pocket formed by several amino acid residues. In particular, Met179, Ala275, Val253, Thr257, Val250, and Met272 are arranged within 3.5 Å around the cyclopentyl ring of CPA. Additionally, the hydroxyl groups of the ligand at the

2′-position forms a water mediated interaction with Leu81, however, the 3′-hydroxyl group of the ligand interacts with His280 (Fig. 8). The results are in accordance with published data regarding the binding modes of the adenosine receptor agonists [59].

The N^6-substituted NECA derivative [60] (compound **5** in Fig. 3) nicely fits inside the TM regions of the model of the A_{2B} receptor. This agonist shows many hydrophilic interactions and interacts in the same manner as NECA (Fig. 8). In addition, the furan moiety of the ligand is in contact with Met272, Ala271, Ala275, Val253, Val250, Met179, and the lipophobic part of Lys267 which is in agreement with mutagenesis studies demonstrating that the said residues exert an effect on agonist affinity (Table 2).

The interaction pattern obtained for the non-nucleosidic A_{2B}-selective agonist BAY 60-6583, [52] which (apart from having a planar heterocyclic core) only distantly resembles the native agonist adenosine or its derivatives (compound **7** in Fig. 3) suggests that the amino group at the 6-position of BAY 60-6583 forms a hydrogen bonding interaction to the amide oxygen of Asn254, and the protonated nitrogen atom of His251 is involved in a hydrogen bonding interaction with the carbonyl group of the sulfanylacetamide moiety of the ligand. Furthermore, the amide side chain of Asn186 makes a hydrogen bonding with the amino group of sulfanylacetamide moiety of the ligand. Also, Gln90 is observed in proximity to the amino group of sulfanylacetamide of the ligand (3.3 Å).

The oxygen atom of the cyclopropylmethyl-phenyl ether of the ligand is within a hydrogen bonding distance of the protonated nitrogen atom of His280 and Ser279 is predicted to be in proximity to the oxygen atom of the cyclopropylmethyl-phenyl ether. The cyano group at the 3-position of the ligand is involved in a hydrogen bonding interaction with Thr89. The cyano group at the 5-position of the ligand forms a water mediated hydrogen bonding interaction.

The phenylpyridine moiety of the ligand is stabilized by an aromatic stacking interaction with Phe173 and located inside in the hydrophobic pocket delimited by Leu86, Met182, Met179, Ala275, Val253, Phe243, Phe187, Val250, Ile276, Val85, and Trp247, while the cyclopropyl residue is surrounded by Leu81, Ile67, Ala82, Phe63 and Ala64 (Fig. 8).

Summarizing here, we may say, that the adenosine agonists, which have a similar (purine) ring structure as the xanthine antagonists (even though the interaction pattern is inverted), analogously present a common binding pattern. As key residues again Asn254 was identified, but now His280 is also constantly involved in contacting the ribose moiety, which is essential for the agonistic character of the compounds investigated so far. The residue of the template structure bovine rhodopsin that corresponds to His280 is Lys296, which is the one that carries the covalently bound *cis–trans* retinal. This implies that His280 might be directly involved in or even triggers the receptor activation mechanism.

Table 7 EC_{50} values and computed ΔG values for all agonists tested (EC_{50} values for NECA and BAY60-6583 are from S. Hinz, A. Schiedel, C. E. Müller, unpublished results)

	Ligand	EC_{50} (nM)	Calculated ΔG (kcal mol^{-1})
1	Adenosine [57]	23,500	−65.06
2	CADO [58]	24,000	−64.64
3	NECA [50]	83.5	−76.01
4	CPA [58]	18,600	−67.84
5	NECA derivative [60]	82	−87.28
6	BAY60-6583 [52]	42.4	−96.11

Again, the geometrical observations were complemented by estimating the strength of the ligand–receptor interactions. The difficulty here was, however, that the agonist effects were measured by functional assays which yield EC_{50} values. Those cannot unambiguously be converted to K_i-values, since they depend very much on test conditions, in particular receptor density. Results from radioligand binding studies of agonists versus an agonist radioligand (labelling the high-affinity state of the receptor) would be ideal for the calculations, but such data are not available since an agonist radioligand has not yet been developed for A_{2B} receptors. Table 7 lists the EC_{50} values obtained in cAMP assays along with computed ΔG values. Since the data were taken from different studies, they can only provide a very rough estimate of compound activity.

According to Table 7 the calculations for the adenosine and non-adenosine agonists reproduced the experimentally observed trends to some degree. Our results contradict the binding modes reported previously in the literature by Ivanov et al. [13], who postulated binding modes for xanthine derivatives that differ significantly from the positions we propose. This is mainly due to an alternate choice of the location of the binding site. Our choice of the binding center relies on the evidence given by the positions of the cocrystallized ligands bound to their template structures, retinal bound to rhodopsin, carazolol bound to the β_2-adrenergic receptor, and ZM241385 bound to the adenosine A_{2A} receptor. The residues identified by our procedure as part of the binding pocket indeed turned out to be relevant for ligand binding in mutagenesis studies for either the A_{2B} receptor directly or the closely related adenosine A_{2A} receptor. Our approach finally allowed us to outline the general trend between the experimentally observed and the computed binding behaviour. The final correlation of the calculated binding affinities with experimental findings justifies in retrospect our initially made, severely simplifying assumption that the natural membrane environment is

dispensable, at least for the limited purpose of this application. Recently, the crystal structure of opsin was published, which displays structural features that are attributed to an active GPCR state [61]. Like our receptor model in complex with the agonist, the opsin shows prominent structural changes in the conserved E(D)RY region.

Conclusions

We have developed and compared a novel 3D model of the human adenosine A_{2B} receptor, based on the highest resolution structures of bovine rhodopsin, of the β_2-adrenergic receptor and of the recently adenosine A_{2A} receptor, incorporating information from mutagenesis studies at the same time. Also, based on the results obtained, possible explanations for the selectivities of the adenosine A_{2A} and A_{2B} receptors were described.

In the course of combined docking and MD simulation studies the model has been thoroughly investigated; the structural effects of ligand binding have been examined on the basis of hydrogen bonds, lipophilic interactions and binding energies in the final complexes obtained from automatic ligand placement and structural refinement. For antagonists, which address the inactive state of the receptor, the outcome was generally in concordance with experimentally conducted binding studies, for agonists, that trigger/require significant changes in the conformation of the receptor, the results were also plausible. Thus, for the receptor ground state the final model not only integrates without any contradictions sequential and structural information, as well as evidence from site-directed mutagenesis and binding studies, rendering a quite plausible model for ligand receptor interactions. Given the profile of sequence similarity, which is highest in the trans-membrane parts, we may consider the helical bundle as comparatively very well characterized in contrast to the intra- and extra-cellular loop regions. The major part of the binding site is made up by the trans-membrane helices; however the exact structure of the second extracellular loop, which may also be involved in ligand binding, is still quite uncertain. We have made suggestions on the potential structure of this part, which will require further confirmation.

Nevertheless, the results of the present study provide valuable information concerning the optimal structural requirements for selective antagonist and agonist recognition by the human adenosine A_{2B} receptor. Most of the amino acid residues covering the putative binding sites are conserved among the four adenosine receptor subtypes. Asn254, His280, Trp247, Leu86, and Ile276, which are common to all subtypes, are believed to play an important role in the binding of both agonists and antagonists. In order to design new, receptor subtype-selective ligands, we need to target the non-conserved amino acid residues that point to the center of the trans-membrane part according to the present study, namely Asn273, Leu81, Lys170, Val256, Ala271, Asn266, Lys269, Lys267 and Val250. These residues are in proximity to the ligand, but specific for the A_{2B} receptor. The actual behaviour of compounds designed on these predictions will help to confirm and optimize the presented receptor model.

References

1. Lagerstrom MC, Schiöth HB (2008) Structural diversity of G protein-coupled receptor and significance for drug discovery. Nat Rev Drug Discov 7:339–357
2. Overington JP, Al-Lazikani B, Hopkins AL (2006) How many drug targets are there? Nat Rev Drug Discov 5(12):993–996
3. Svoboda P, Teisinger J, Novotny J, Bourova L, Drmota T, Hejnova L, Moravcova Z, Lisy V, Rudajev V, Stöhr J, Vokurkova A, Svandova I, Durchankova D (2004) Biochemistry of transmembrane signalling mediated by trimeric G proteins. Physiol Res 53:S141–S152
4. Böhm HJ, Klebe G, Kubinyi H (1996) Wirkstoffdesign Der Weg zum Arzneimittel, 1st edn. Spektrum Akademischer Verlag, Heidelberg. ISBN 13:978-3827413536
5. Fredholm BB, Abbracchio MP, Burnstock G, Dubyak GR, Harden TK, Jacobson KA, Schwabe U, Williams M (1997) Towards a revised nomenclature for P1 and P2 receptors. Trends Pharmacol Sci 18:79–82
6. Fredholm BB, IJzerman AP, Jacobson KA, Klotz K-N, Linden J (2001) International Union of Pharmacology. XXV. Nomenclature and classification of adenosine receptors. Pharmacol Rev 53:527–552
7. Müller CE, Stein B (1996) Adenosine receptor antagonists: structures and potential therapeutic applications. Curr Pharm Design 2:501–530
8. Müller CE (2000) Adenosine receptor ligands: recent developments part I. Agonists. Curr Med Chem 7:1269–1288
9. Grenz A, Osswald H, Eckle T, Yanq D, Zhang H, Tran ZV, Klingel K, Ravid K, Eltzschig HK (2008) The reno-vascular A_{2B}adenosine receptor protects the kidney from ischemia. PLoS Med 5:e137
10. Volpini R, Costanzi S, Vittori S, Cristalli G, Klotz KN (2003) Medicinal chemistry and pharmacology of A_{2B} adenosine receptors. Curr Top Med Chem 3:427–443
11. Holgate ST (2005) the Quintiles Prize Lecture 2004. The identification of the adenosine A_{2B} receptors as a novel therapeutic target in asthma. Br J Pharmacol 145:1009–1015
12. Palczewski K, Kumasaka T, Hori T, Behnke CA, Motoshima H, Fox BA, Le Trong I, Teller DC, Okada T, Stenkamp RE, Yamamoto M, Miyano M (2000) Crystal structure of rhodopsin: a G protein-coupled receptor. Science 289:739–745
13. Ivanov AA, Baskin II, Palyulin VA, Piccagli L, Baraldi PG, Zefirov NS (2005) Molecular modeling and molecular dynamics simulation of the human A_{2B} adenosine receptor. The study of the possible binding modes of the A_{2B} receptor antagonists. J Med Chem 48:6813–6820
14. Okada T, Sugihara M, Bondar AN, Elstner M, Entel P, Buss V (2004) The retinal conformation and its environment in rhodopsin in light of a new 2.2 Å crystal structure. J Mol Biol 342:571–583
15. Cherezov V, Rosenbaum DM, Hanson MA, Rasmussen SG, Thian FS, Kobilka TS, Choi HJ, Kuhn P, Weis WI, Kobilka BK,

Stevens RC (2007) High resolution crystal structure of an engineered human ß$_2$-adrenergic G protein-coupled receptor. Science 318:1258–1265
16. Jaakola V-P, Griffith MT, Hanson MA, Cherezov V, Chien EYT, Lane JR, IJzerman AP, Stevens RC (2008) The 2.6 Angstrom crystal structure of a human A_{2A} adenosine receptor bound to an antagonist. Science 322(5905):1211–1217
17. Fersht A (1985) Enzyme structure and mechanism, 2nd edn. Freeman, New York, p 6
18. Forrest LR, Tang CL, Honig B (2006) on the accuracy of homology modeling and sequence alignment methods applied to membrane proteins. Biophys J 91:508–517
19. Radestock S, Weil T, Renner S (2008) Homology model-based virtual screening for GPCR ligands using docking and target-biased scoring. J Chem Inf Model 48:1104–1117
20. Ferrara P, Jacoby E (2007) Evaluation of the utility of homology models in high throughput docking. J Mol Model 13:897–905
21. Kairys V, Fernandes MX, Gilson MK (2006) Screening drug-like compounds by docking to homology models: a systematic study. J Chem Inf Model 46:365–379
22. Bairoch A, Apweiler R (2000) The SWISS-PROT protein sequence database and its supplement TrEMBL. Nucleic Acids Res 28:45–48
23. Thompson JD, Gibson TJ, Plewniak F, Jeanmougin F, Higgins DG (1997) The CLUSTAL: X windows interface: flexible strategies for multiple sequence alignment aided by quality analysis tools. Nucleic Acids Res 25:4876–4882
24. Fredriksson R, Lagerström MC, Lundin L-G, Schiöth HB (2003) Mol Pharm 63:1256–1272
25. Imai T, Fujita N (2004) Statistical sequence analyses of G-protein-coupled receptors: structural and functional characteristics viewed with periodicities of entropy, hydrophobicity, and volume. Proteins Struct Funct Bioinf 56:650–660
26. Ballesteros JA, Weinstein HW (1995) Integrated methods for the construction of three-dimensional models and computational probing of structure–function relation of G protein-coupled receptors. Methods Neurosci 25:366–428
27. Canutescu AA, Shelenkov AA, Dunbrack RL Jr (2003) A graph-theory algorithm for rapid protein side-chain prediction. Protein Sci 212:2001–2014
28. Pearlman DA, Case DA, Caldwell JW, Ross WS, Cheatham TE, Debolt S, Ferguson D, Seibel G, Collman P (1995) AMBER, a package of computer-programs for applying molecular mechanics, normal-mode analysis, molecular-dynamics and free-energy calculations to simulate the structural and energetic properties of molecules. Comput Phys Commun 91:1–41
29. Rarey M, Kramer B, Lengauer T, Klebe G (1996) Prediction receptor–ligand interaction by an incremental construction algorithm. J Mol Biol 261:470–489
30. Rarey M, Kramer B, Lengauer T (1997) Multiple automatic base selection: protein–ligand docking based on incremental construction without manual intervention. J Comp Aided Mol Des 11:369–384
31. Åquist J (1996) Calculation of absolute binding free energies for charged ligands and effects of long range electrostatic interactions. J Comp Chem 17:1587–1597
32. Kuhn B, Kollman PA (2000) Binding of a diverse set of ligands to avidin and streptavidin: an accurate quantitative prediction of their relative affinities by a combination of molecular mechanics and continuum solvent models. J Med Chem 43:3786–3791
33. Wang J, Dixon R, Kollmann PA (1999) Ranking ligand binding affinities with avidin: a molecular dynamics-based interaction energy study. Proteins 34:69–81
34. Schlegel B, Sippl W, Höltje H–D (2005) Molecular dynamics simulations of bovine rhodopsin: influence of protonation states and different membrane-mimicking environments. J Mol Model 12:49–64
35. Bockaert J, Pin JP (1999) Molecular tinkering of G protein-coupled receptors: an evolutionary success. EMBO J 18:1723–1729
36. Pospisil P, Folkers G (2004) Making the best account of molecular docking in drug design. J Pharm Sci 29:81–92
37. Rosenbaum DM, Cherezov V, Hanson MA, Rasmussen SG, Thian FS, Kobilka TS, Choi HJ, Yao XJ, Weis WI, Stevens RC, Kobilka BK (2007) GPCR Engineering yields high-resolution structural insights into β_2-adrenergic receptor function. Science 318:1266–1273
38. Schlegel B, Laggner C, Meier R, Langer T, Schnell D, Seifert R, Stark H, Höltje HD, Sippl W (2007) Generation of a homology model of the human histamine H3 receptor for ligand docking and pharmacophore-based screening. J Comput Aided Mol Des 21(8):437–454
39. Rockey WM, Elcock AH (2006) Structure selection for protein kinase docking and virtual screening: homology models or crystal structures? Curr Protein Pept Sci 7:437–457
40. Laskowski RA, MacArthur MW, Moss DS, Thornton JM (1993) PROCHECK: a program to check the stereochemical quality of protein structures. J Appl Cryst 26:283–291
41. Morris AL, MacArthur MW, Hutchinson EG, Thornton JM (1992) Stereochemical quality of protein structure coordinates. Proteins 12:345–364
42. Sippl MJ (1993) Recognition of errors in three-dimensional structures of proteins. Proteins 17:355–362. http://www.came.sbg.ac.at/
43. Ongini E, Dionisotti S, Gessi S, Irenius E, Fredholm BB (1999) Comparison of CGS15943, ZM241385 and Sch58261 as antagonists at human adenosine receptors. Naunyn–Schmiedeberg's Arch Pharmacol 359:7–10
44. Sauer R, Maurinsh J, Reith U, Fülle F, Klotz KN, Müller CE (2000) Water-soluble phosphate prodrugs of 1-propargyl-8-styrylxanthine derivatives, A_{2A}-selective adenosine receptor antagonists. J Med Chem 43:440–448
45. Knutsen LJ, Weiss SM (2001) KW-6002 (Kyowa Hakko Kogyo). Curr Opin Invest Drugs 2:668–673
46. Hodgson RA, Bertorelli R, Varty GB, Lachowicz JE, Forlani A, Fredduzzi S, Cohen-Williams ME, Higgins GA, Impagnatiello F, Nicolussi E, Parra LE, Foster C, Zhai Y, Neustadt BR, Stamford AW, Parker EM, Reggiani A, Hunter JC (2009) Characterization of the potent and highly selective A_{2A} receptor antagonists preladenant and SCH412348 in rodent models of movement disorders and depression. J Pharmacol Exp Ther. doi: 10.1124/jpet.108.149617
47. Kim YC, Ji XD, Melman N, Linden J, Jacobson KA (2000) Anilide derivatives of an 8-phenylxanthine carboxylic congener are highly potent and selective antagonists at human A_{2B} adenosine receptor. J Med Chem 43:1165–1172
48. Baraldi PG, Tabrizi MA, Preti D, Bovero A, Romagnoli R, Fruttarolo F, Zaid NA, Moorman AR, Varani K, Gessi S, Merighi S, Borea PA (2004) Design, synthesis, and biological evaluation of new 8-heterocyclic xanthine derivatives as highly potent and selective human A_{2B} adenosine receptor antagonists. J Med Chem 47:1434–1447
49. Yan L, CG BertarelliD, Hayallah AM, Meyer H, Klotz K-N, Müller CE (2006) A new synthesis of sulfonamides by aminolysis of p-Nitrophenylsulfonates yielding potent and selective adenosine A_{2B} receptor antagonists. J Med Chem 49:4384–4391
50. Gao ZG, Mamedova LK, Chen P, Jacobson KA (2004) 2-Substituted adenosine derivatives: affinity and efficacy at four subtypes of human adenosine receptors. Biochem Pharmacol 68:1985–1993

51. Jarvis MF, Schulz R, Hutchison AJ, Do UH, Sills MA, Williams M (1989) [3H] CGS21680, a selective A2 adenosine receptor agonist directly labels A2 receptor in rat brain. J Pharmacol Exp Ther 251:888–893
52. Eckle T, Krahn T, Grenz A, Köhler D, Mittelbronn M, Ledent C, Jacobson MA, Osswald H, Thompson LF, Unertl K, Eltzschig HK (2007) Cardioprotection by ecto-5′-nucleotidase (CD73) and A_{2B} adenosine receptors. Circulation 115:1581–1590
53. Kim SA, Marshall MA, Melman N, Kim HS, Müller CE, Linden J, Jacobson KA (2002) Structure–activity relationships at human rat A_{2B} adenosine receptors of xanthine derivatives substituted at the 1-, 3-, 7-, and 8-positions. J Med Chem 45:2131–2138
54. Hayallah AM, Sandoval-Ramirez J, Reith U, Schobert U, Preiss B, Schumacher B, Daly JW, Müller CE (2002) 1, 8-Disubstituted xanthine derivatives: synthesis of potent A_{2B} selective adenosine receptor antagonists. J Med Chem 45:1500–1510
55. Vidal B, Nueda A, Esteve C, Domench T, Benito S, Reinoso RF, Pont M, Calbet M, Lopez R, Cadavid MI, Loza MI, Cardenas A, Godessart N, Beleta J, Warrellow G, Ryder H (2007) Discovery and characterization of 4′-(2-furyl)-N-pyridin-3-yl-4,5′-bipyrimidin-2′-amine (LAS38096), a potent, selective, and efficacious A_{2B} adenosine receptor antagonist. J Med Chem 50:2732–2736
56. Stewart M, Steinig AG, Ma C, Song JP, McKibben B, Castelhano AL, MacLennan SJ (2004) [^{3}H]OSIP339391, a selective, novel, and high affinity antagonist radioligand for adenosine A_{2B} receptors. Biochem Pharmacol 68:305–312
57. Vittori S, Camaioni E, Costanzi S, Volpini R, Klotz KN, Cristalli G (1999) Synthesis and receptor affinity of polysubstituted adenosine. Nucleosid Nucleotid 18:739–740
58. Klotz KN, Hessling J, Hegler J, Owman C, Kull B, Fredholm BB, Lohse MJ (1998) Comparative pharmacology of human adenosine receptor subtypes characterization of stably transfected receptors in CHO cells. Naunyn-Schmiedeberg's Arch Pharmacol 357:1–9
59. Ivanov AA, Palyulin VA, Zefirov NS (2007) Computer aided comparative analysis of the binding modes of the adenosine receptor agonists for all known subtypes of adenosine receptors. J Mol Graphics Model 25:740–754
60. Baraldi PG, Preti D, Tabrizi MA, Fruttarolo F, Romagnoli R, Carrion MD, Cara LCL, Moorman AR, Varani K, Borea PA (2007) Synthesis and biological evaluation of novel 1-deoxy-1-[6-[((hetero)arylcarbonyl)hydrazino]-9H-purin-9-yl]-N-ethyl-β-D-ribofuranuronamide derivatives as useful templates for the development of A_{2B} adenosine receptor agonists. J Med Chem 50:374–380
61. Park JH, Scheerer P, Hofmann KP, Choe H-W, Ernst OP (2008) Crystal structure of the ligand-free G protein-coupled receptor opsin. Nature 454:07063
62. IJzerman AP, Von Frijtag Drabbe Künzel JK, Kim J, Jiang Q, Jacobson KA (1996) Site-directed mutagenesis of the human adenosine A_{2A} receptor. Critical involvement of Glu13 in agonist recognition. Eur J Pharmacol 310:269–272
63. Beukers MW, den Dulk H, van Tilburg EW, Brouwer J, IJzerman AP (2000) Why are A_{2B} receptors low-affinity adenosine receptors? Mutation of Asn273 to Tyr increases affinity of the human A_{2B} receptor for 2-(1-hexynyl) adenosine. Mol Pharmacol 58:1349–1356
64. Jiang Q, Lee BX, Glashofer M, van Rhee AM, Jacobson KA (1997) Mutagenesis reveals structure–activity parallels between human A_{2A} adenosine receptors and biogenic amine G protein-coupled receptors. J Med Chem 40:2588–2595
65. Jiang Q, van Rhee AM, Kim J, Yehle S, Wess J, Jacobson KA (1996) Hydrophilic side chains in the third and seventh transmembrane helical domains of human A_{2A} adenosine receptor are required for ligand recognition. Mol Pharmacol 50:512–521
66. Beukers MW, van Oppenraaij J, van der Hoorn PP, Blad CC, den Dulk H, Brouwer J, IJzerman AP (2004) Random mutagenesis of the human adenosine A_{2B} receptor followed by growth selection in yeast, identification of constitutively active and gain of function mutations. Mol Pharmacol 65:702–710
67. Kim J, Jiang Q, Glashofer M, Yehle S, Wees J, Jacobson KA (1996) Glutamate residues in the second extracellular loop of the human A_{2A} adenosine receptor are required for ligand recognition. Mol Pharmacol 49:683–691
68. Kim J, Wess J, van Rhee AM, Schöneberg T, Jacobson KA (1995) Site-directed mutagenesis identifies residues involved in ligand recognition in the human A_{2A} adenosine receptor. J Biol Chem 270:13987–13997
69. Gao Z-G, Jiang Q, Jacobson KA, IJzerman AP (2000) Site-directed mutagenesis studies of human A_{2A} adenosine receptors: involvement of Glu13 and His278 in ligand binding and sodium modulation. Biochem Pharmacol 60:661–668